Fuel 310 (2022) 122113

Contents lists available at ScienceDirect

Fuel

journal homepage: www.elsevier.com/locate/fuel

Flexible Power & Biomass-to-Methanol plants: Design optimization and economic viability of the electrolysis integration

Alessandro Poluzzi [a], Giulio Guandalini [a], Simone Guffanti [a], Cristina Elsido [a], Stefania Moioli [b], Patrick Huttenhuis [c], Glenn Rexwinkel [c], Emanuele Martelli [a], Gianpiero Groppi [a], Matteo C. Romano [a,*]

[a] Politecnico di Milano, Dipartimento di Energia, Via Lambruschini 4, 20156 Milano, Italy
[b] Politecnico di Milano, Dipartimento di Chimica, Materiali e Ingegneria Chimica "Giulio Natta", Piazza Leonardo da Vinci 32, 20133 Milano, Italy
[c] Frames Renewable Energy Solutions BV, Eikenlaan 237, 2404 BP Alphen aan den Rijn, the Netherlands

ARTICLE INFO

Keywords:
Biomass
Methanol
E-methanol
E-fuel
Hydrogen
Power-to-X

ABSTRACT

This paper assesses the optimal design criteria of a flexible power and biomass to methanol (PBtM) plant, conceived to operate both without green hydrogen addition (baseline mode) and with hydrogen addition (enhanced mode), following an intermittent use of the electrolysis system, which is turned on when the electricity price allows an economically viable hydrogen production. The assessed plant includes a gasification section, syngas cleaning and compression, methanol synthesis and purification and heat recovery steam cycle, to be flexibly operated. A sorption-enhanced gasification technology allows to produce a tailored syngas for the downstream synthesis in both the baseline and enhanced operating conditions, by controlling the in-situ CO_2 separation rate. Two designs are assessed for the methanol synthesis unit, with two different reactor sizes: (i) a larger reactor, designed on the enhanced operation mode (enhanced reactor design – ERD) and (ii) a smaller reactor, designed on the baseline operation mode (baseline reactor design – BRD). The ERD design resulted to be preferable from the techno economic perspectives, resulting in 20% lower cost of the e-MeOH (30.80 vs. 37.76 €/GJ_{LHV}) with the baseline assumptions (i.e. 80% of electrolyzer capacity factor and 2019 Denmark day-ahead market electricity price). Other important outcomes are: (i) high electrolysis capacity factor is needed to obtain competitive cost of e-MeOH and (ii) advantages of flexibly operated PBtM plants with respect to inflexible PBtM plants are significant in scenarios with high penetration of intermittent renewables, leading to low average prices of electricity but also longer periods of high peak prices.

1. Introduction

Liquid biofuels represent a valuable option for the decarbonization of heavy-duty road and off-road vehicles, shipping and aviation due to the significant challenges in the electrification of these sectors. Biofuels are also suitable for reducing CO_2 emissions from light duty vehicles in the transition to electric and hydrogen-based mobility. In the coming decades, an increased share of advanced biofuels from low-risk ILUC (indirect land use change) feedstocks is expected and required by regulations [1]. Increasing the economic competitiveness of advanced biofuels is key for their wide deployment. The current estimated costs of advanced biofuels lie in the range of 17–44 €/GJ for biomass-based production and of 13–29 €/GJ for waste-based production, while the fossil fuel production cost varies between 8 and 14 €/GJ [2]. New opportunities for biofuels may derive from the integration with electrolyzers, generating hydrogen to be combined with the carbon-rich syngas from biomass gasification. The potential benefit of such power & biomass-to-X (PBtX) concept is twofold: (i) to increase the utilization of the biogenic carbon in the biomass, enhancing the production of high value bio-product for a given size and cost of the biomass supply chain, pretreatment and gasification equipment and (ii) to provide services to the electric grid through power-to-X energy storage.

In the literature, a number of plant configurations including different gasification technologies, conditioning units and biofuels have been assessed (see Table 1). Also, different types of electrolysis technologies can be integrated with Biomass-to-X (BtX) processes, implying different levels of flexibility of the overall plant.

Hannula [3] examined the co-production of synthetic natural gas, methanol or gasoline (MTG) from biomass residues and electricity. The

* Corresponding author.
E-mail address: matteo.romano@polimi.it (M.C. Romano).

https://doi.org/10.1016/j.fuel.2021.122113
Received 2 April 2021; Received in revised form 23 July 2021; Accepted 23 September 2021
Available online 20 November 2021

Nomenclature

Acronyms

AGR	Acid gas removal
ASU	Air separation unit
ATR	Autothermal reformer
BFB	Bubbling fluidized bed
BO	Baseline operation
BRD	Baseline reactor design
BtM	Biomass-to-Methanol
BtX	Biomass-to-X
BWR	Boiling water reactor
CFB	Circulating fluidized bed
CZA	Methanol synthesis catalyst $Cu/ZnO/Al_2O_3$
DME	Dimethyl ether
EO	Enhanced operation
ERD	Enhanced reactor design
GHSV	Gas hourly space velocity
HEN	Heat exchanger network
HP	High pressure level
HRSC	Heat recovery steam cycle
ICE	Internal combustion engine
ILUC	Indirect land use change
JF	Jet fuel
LHV	Lower heating value
LP	Low-pressure level
M	Methanol
MINLP	Mixed integer nonlinear programming
MP	Medium-pressure level
MTG	Methanol-to-gasoline
PBtM	Power & Biomass-to-Methanol
PBtX	Power & Biomass-to-X
PtX	Power-to-X
RR	Recycle ratio
RWGS	Revers water gas shift
SEG	Sorption-enhanced gasification
SNG	Synthetic natural gas
SOEC	Solid oxide electrolyzer cell
WGS	Water gas shift

Symbols

$C_{feedstock}$	Cost of feedstock
$C_{fixedO\&M}$	Fixed O&M cost
C_{ut}	Utilities cost
C_{tot}	Total cost
CE	Carbon efficiency
CF_{el}	Electrolyzer capacity factor
CCF	Capital charge factor
E	Delivered-equipment cost
$F_{C,biom}$	Carbon molar flow rate in the inlet biomass
$F_{fuel,max,i}$	Maximum fuel production
F_i	Component – i molar flow rate
f_i	Multiplying factors for estimating the total capital investment
F_M	Methanol molar flow rate
F_M	Methanol molar flow rate
FCI	Fixed-capital investment
G_S	Solid mass flow per cross-section unit
h_{eq}	Equivalent yearly operating hours
k_i	Parameter – i for ICE performance map
K_p	Equilibrium constant
IRR	Internal rate of return
L	ICE load as thermal input power
$LCOF$	Levelized cost of fuel
LT	Plant lifetime
$\dot{m}_{es}$	Entrained solids mass flow rate
$\dot{m}_{gas}$	Gas mass flow rate
$\dot{m}_i$	Component – i mass flow rate
M_{tot}	Amount of fuel
NPV	Net present value
P	ICE electric power output
$p_{\delta_{WGS}}$	Approach to the WGS equilibrium composition
P_{el}	Net electric output
PCE	Potential carbon efficiency
p_i	Partial pressure of the species – i
S	ICE size
TCI	Total capital investment cost
v_{gas}	Gas velocity
ν_i	Stoichiometric coefficient – i
WC	Working capital
WTP_{ST}	Short-term willingness to pay
α	Discount rate
$\eta_{el,ref}$	Reference steam cycle electric efficiency
$\eta_{F,dry}$	Dryer fuel efficiency
$\eta_{F,SEG}$	SEG fuel efficiency
$\eta_{F,ref}$	Reformer fuel efficiency
$\eta_{F,pur}$	Purification fuel efficiency
η_{F,M_syn}	Methanol synthesis fuel efficiency
η_{F,M_pur}	Methanol purification fuel efficiency
$\eta_{F,global}$	Global fuel efficiency
$\eta^u_{F,i}$	Useful fuel efficiency of the – i unit
$\eta_{F,eq}$	Equivalent fuel efficiency
η_{HtF}	Hydrogen-to-fuel efficiency
η_{PtF}	Power-to-fuel efficiency
χ_C	Number of carbon atoms in the product molecule
ρ_{gas}	Gas density

biomass feedstock is gasified with an oxygen-blown fluidized bed reactor. The BtX plants employ a water gas shift (WGS) reactor for the control of the syngas composition. When hydrogen is added to the system, the WGS is bypassed. The acid gas removal (AGR) unit separates 98% of the CO_2 contained in the syngas independently on whether green hydrogen is added or not. The article compares PBtX, BtX and PtX plant configurations from a techno-economic point of view. The production cost for all the configurations are computed at fixed electricity price and annual operating hours. The economic competitiveness of operating the PBtX plant flexibly is assessed with a simplified approach, by computing the breakeven electricity price at different annual operating hours that guarantees a profitable operation with respect to the reference BtX plant.

Hannula [4] and Koponen et al. [5] studied how to increase biofuels production from given amount of biomass by feeding external hydrogen from alkaline water electrolysis to a gasification-based biorefinery. Two gasification alternatives, i.e. oxygen blown and indirect gasification, and two different end-product alternatives, i.e. synthetic gasoline via methanol and synthetic natural gas, are assessed. In the PBtX plants, the CO_2 contained in the syngas is not separated and it is used as feedstock for the synthesis. The operational flexibility is not considered, therefore the PBtX plants imply a continuous external hydrogen supply and neither the WGS reactor nor the AGR unit for CO_2 separation are necessary. The study compares PBtX and BtX plant configurations from the techno-economic perspectives. The production costs are calculated at given electricity price and annual operating hours. The breakeven

Table 1
Selected studies on Power & Biomass-to-X plants.

Reference	Gasification technology	Syngas cleaning and conditioning processes	Electrolyser technology	Biofuel produced	Carbon efficiency[1]	PtX efficiency[1,2]	HtX efficiency[1]	Economic assumptions	Production cost[1]
Hannula 2015 [3]	Oxygen-blown (fluidized bed)	Reformer (downstream gasifier), WGS reactor, CO_2 separation	Alkaline	M, SNG, MTG	BtX: 37.5% (M) 32.2% (MTG) 33.1% (SNG) PBtX: 48.9% (M) 42.1% (MTG) 49.8% (SNG)	51.7% (M) 44.6% (MTG) 51.1% (SNG)	84.7% (M) 73.1 (MTG) 82.3% (SNG)	Electrolysis cost: 589 €/kW (M) 571 €/kW (MTG) 565 €/kW (SNG) Electricity price: 50.4 €/MWh Electrolysis CF: 91% (8000 h/y) Biomass cost: 5 €/GJ TCI (per kW_{prod}): 2320 €/kW (M) 3050 €/kW (MTG) 1925 €/kW (SNG)	24.4 €/GJ (M) 27.6 €/GJ (MTG) 22.7 €/GJ (SNG)
Hannula 2016 [4], Koponen et al. 2017 [5]	Oxygen-blown (fluidized bed)	Reformer (downstream gasifier)	Alkaline	MTG, SNG	BtX: 30.5% (MTG) 32.5% (SNG) PBtX: 79.4% (MTG) 98.0% (SNG)	48.4% (MTG) 55.1% (SNG)	72.2% (MTG) 82.3% (SNG)	Electrolysis cost: - Electricity price: 50.4 €/MWh Electrolysis CF: 91% (8000 h/y) Biomass cost: 5 €/GJ TCI (per kW_{prod}): 2030 €/kW (MTG) 925 €/kW (SNG)	31.3 €/GJ (MTG) 21.4 €/GJ (SNG)
Hannula 2016 [4], Koponen et al. 2017 [5]	Indirect (dual fluidized bed)	Reformer (downstream gasifier)	Alkaline	MTG, SNG	BtX: 28.8% (MTG) 31.4% (SNG) PBtX: 58.4% (MTG) 67.0% (SNG)	49.7% (MTG) 55.0% (SNG)	74.2% (MTG) 82.1% (SNG)	Electrolysis cost: - Electricity price: 50.4 €/MWh Electrolysis CF: 91% (8000 h/y) Biomass cost: 5 €/GJ TCI (per kW_{prod}): 2551 €/kW (MTG) 1287 €/kW (SNG)	30.4 €/GJ (MTG) 20.4 €/GJ (SNG)
Albrecht et al. 2017 [6]	Pyrolysis + entrained flow	RWGS	PEM	F-T fuels	BtX: 24.9% PBtX: 97.7%	58.2%	83.1%	Electrolysis cost: 942 €/kW Electricity price: 105 €/MWh Electrolysis CF: 94% (8260 h/y) Biomass cost: 5.4 €/GJ TCI (per kW_{prod}): 5559 €/kW	67.2 €/GJ[3] 70.0 €/GJ
Hillestad et al. 2018 [7]	Torrefaction + entrained flow	RWGS, CO_2 separation	SOEC	F-T fuels	BtX: 37.8% PBtX: 91.3%	78.6%	82.4%	Electrolysis cost: 893 €/kW Electricity price: 44.6 €/MWh Electrolysis CF: 89% (7800 h/y) Biomass cost: 3.6 €/GJ TCI (per kW_{prod}): 4212 €/kW	45 €/GJ

(*continued on next page*)

Table 1 (*continued*)

Reference	Gasification technology	Syngas cleaning and conditioning processes	Electrolyser technology	Biofuel produced	Carbon efficiency[1]	PtX efficiency[1,2]	HtX efficiency[1]	Economic assumptions	Production cost[1]
Zhang et al. 2020 [8]	Entrained flow	–	SOEC	SNG, M, DME, JF	BtX: 27.7% (SNG) 35.6% (M) 36.1 (DME) PBtX: 85.4% (SNG) 85.9% (M) 86.3% (DME)	75.3% (SNG) 79.8% (M) 81.8% (DME) 68.3% (JF)	N/A	Electrolysis cost: N/A Electricity price: 61.9 €/MWh Electrolysis CF: 82% (7200 h/y) Biomass cost: 5.1 €/GJ TCI (per kW_{prod})[5]: 1871 €/kW (SNG) 1747 €/kW (M) 1962 €/kW (DME) 3288 €/kW (JF)	25.4–20.3 €/GJ (SNG)[6] 28.0–22.0 €/GJ (M)[6] 31.4–23.7 €/GJ (DME)[6] 50.0–33.1 €/GJ (JF)[6]
Zhang et al. 2020 [8]	Entrained flow	WGS reactor, CO_2 separation	SOEC co-electrolysis	SNG, M, DME, JF	BtX: 27.7% (SNG) 35.6% (M) 36.1 (DME) PBtX: 86.7% (SNG) 85.0% (M) 66.6% (DME)	75.3% (SNG) 76.6% (M) 48.5% (DME)[4] 63.4% (JF)	N/A	Electrolysis cost: N/A Electricity price: 61.9 €/MWh Electrolysis CF: 82% (7200 h/y) Biomass cost: 5.1 €/GJ TCI (per kW_{prod})[7]: N/A	28.0–22.0 €/GJ (SNG)[6] 30.5–23.7 €/GJ (M)[6] 40.7–31.4 €/GJ (DME)[6] 58.5–38.1 €/GJ (JF)[6]

[1] Most of the values derive from computations from the data in the papers. Fuel properties values come from [10] (e.g. LHV, MM, density etc.), when not present in the reference. When necessary, the 2019 conversion $/€ equal to 1.12 has been applied.
[2] The PtX efficiency is computed by taking into account the electricity consumption of the electrolysis system.
[3] Revenues from heat export are taken into account.
[4] Due to additional heat demand. See the reference for more details.
[5] For biomass plant capacity of 60 MW_{LHV}.
[6] For biomass plant capacity of 10–60 MW_{LHV}.
[7] Similar to the previous row Zhang et al. 2020 [8].

hydrogen price is calculated so as to obtain the same fuel production cost in BtX and PBtX configurations.

Albrecht et al. [6] proposed the co-production of F-T fuels from biomass gasification and hydrogen addition from PEM electrolysis, which offers the potential to connect the device directly to fluctuating power sources thanks to its superior dynamic operation behavior. By choosing this type of electrolysis technology, the plant can operate more flexibly, although the flexibility is not explored within the article. The raw syngas from entrained flow biomass gasification is enriched with hydrogen upstream the RWGS reactor. The PBtX plant is compared with the conventional BtX process which includes both the WGS reactor and the AGR unit for CO_2 removal and with a PtX process. The fuel production cost is computed at fixed electricity price and annual operating hours.

Hillestad et al. [7] presented a PBtX process for the production of Fischer-Tropsch (F-T) liquid fuels where external hydrogen is produced through high temperature steam electrolysis in a solid oxide electrolysis cell (SOEC). The extra hydrogen is mixed with the syngas both at high temperature to convert CO_2 into CO in a reverse water gas shift (RWGS) reactor and at low temperature in order to increase the H_2/CO ratio. SOEC requires less electrical power than alkaline water electrolysis, leading to high PtX efficiency, as shown in Table 1. However, the flexibility of the plant is limited because of the high operating temperature which is not compatible with intermittent operations. The PBtX plant is compared with a conventional BtX process which includes a WGS reactor and an AGR unit for CO_2 removal. The fuel production cost shown in Table 1 is calculated by fixing the electricity price, the annual operating hours and an optimistic investment cost for the SOEC.

Zhang et al. [8] assessed two PBtX concepts with SOEC steam electrolysis and co-electrolysis, respectively. The first concept operates the SOEC with steam electrolysis which produces hydrogen and allows to avoid the WGS reactor and the AGR, aiming at very high carbon utilization. The second concept operates the SOEC with co-electrolysis by converting the CO_2 separated from the syngas. It aims at overcoming the flexibility limitations imposed by the SOEC through a configuration where the electrolyzer does not affect the syngas conditioning process. When renewable electricity is not available, the CO_2 is captured from the syngas and stored, to be converted when renewable electricity becomes available. In the first operating mode, syngas is conditioned through the WGS reactor and CO_2 separation, while in the latter both the units are bypassed. The production cost of the PBtX plants is highly dependent on the price and the availability of renewable electricity. The concept with co-electrolysis allows for additional operational flexibility without renewable electricity, resulting in higher annual production than the steam electrolysis concept, which interrupts the plant operation when renewable electricity is not available. The advantage of the steam electrolysis concept (see Table 1) is overcome by the co-electrolysis configuration in case of limited availability of renewable electricity along the year.

It is noteworthy, that the integration of an electrolysis system offers the opportunity of exploiting the coproduction of oxygen, to be used in the gasification process. On this respect, different criteria may be adopted to size the electrolysis unit, as assessed by Koytsoumpa et al. [9], either to completely satisfy the plant oxygen demand or to retain the maximum amount of carbon in the final product.

In this work, the flexible power and biomass to methanol plant shown in Fig. 1 is assessed, using a low temperature electrolysis technology. The plant is based on a sorption-enhanced gasification (SEG) process, an indirect gasification system with in-situ CO_2 separation by CaO-based sorbent. Following the idea presented in [11], the SEG unit is operated flexibly by controlling the solids circulation rate in order to adjust CO_2 separation in the gasifier and produce a syngas with tailored composition for the downstream synthesis process [12–14]. The proposed system simplifies the syngas conditioning section through process intensification, by avoiding the water gas shift reactor and the CO_2 separation unit. Moreover, the gasification process can be operated flexibly by adapting the sorbent CO_2 uptake on the availability of intermittent hydrogen to be added upstream the methanol synthesis unit.

In addition to the originality of the proposed plant configuration, this paper introduces the following main novelties compared to the existing literature in the calculation approach of PBtX plants:

- the economic optimal design of the plant components depends on the number of hours that the plant is expected to operate without hydrogen addition (baseline operation) and with hydrogen addition (enhanced operation), that are closely related to the variability of the electricity price. In this paper, the optimal design criteria of all the plant components are provided on the basis of the two operating points. Furthermore, two design criteria are compared for the methanol synthesis section, which is sized on the flow rates of either the baseline operation mode or of the enhanced operation mode;
- the plants designed with the two above-mentioned criteria are calculated considering the off-design operation of the main process units, especially of the gasification island, of the heat recovery steam cycle and of the methanol synthesis and purification units;
- an economic analysis is carried out to compare the two design criteria. In this analysis, the link between the methanol selling price, the electricity price and the number of operating hours in enhanced operation is computed through the willingness to pay approach [15], that takes into account the shape of the cumulative electricity price curve.

In the next sections, first, a technical analysis is conducted by discussing the aforementioned ideas. Then, a differential economic analysis is performed in order to evaluate the feasibility and the economic viability of the electrolyzer installation. The economic competitiveness of the flexible Power & Biomass-to-Methanol (PBtM) plant is computed with respect to a Biomass-to-Methanol (BtM) plant. The analysis is conducted by computing the e-Methanol production cost and the plant profitability when coupled with the electric market.

2. Bio-methanol plant description

The block diagram of the plant is shown in Fig. 1 and the stream properties are displayed in Table 2 and 3 for baseline and enhanced operation, respectively. More detailed plant flowsheet and stream properties are included in the supporting information.

As-received woody biomass (stream 1) is fed to a belt dryer to reduce the moisture content from 45% to 15%. The dried biomass (stream 2) is sent to the fluidized bed gasifier, in which the gasification reaction takes place together with the removal of carbon dioxide through carbonation reaction ($CaO + CO_2 \leftrightarrow CaCO_3$). The produced $CaCO_3$ and the residual char are then transferred from the gasifier to the combustor fluidized bed. Here, the combustion of the char and of additional biomass provides the energy required for heating the solids and decomposing calcium carbonate back into calcium oxide. The circulation of hot solids from the combustor to the gasifier allows to thermally sustain the gasification process, through both the sensible heat of the circulating solids and the heat of the carbonation reaction. Solids circulation is tuned to achieve a target CO_2 uptake, which is controlled by the equilibrium of the carbonation reaction. Therefore, by increasing the solids circulation rate, the gasifier temperature increases and the CO_2 separation reduces. In this way, it is possible to obtain a tailored syngas with a target module $M = (H_2 - CO_2)/(CO + CO_2)$, with no need of downstream WGS and CO_2 separation sections.

The SEG process allows to produce a nitrogen-free syngas with tailored carbon content (stream 5) which however contains a significant amount of methane and tar. Since methane is inert in the downstream methanol synthesis process, a catalytic auto-thermal reformer (ATR) unit is included downstream the gasifier and after high temperature filtration to convert methane and tar into CO and H_2. Oxygen (stream 6)

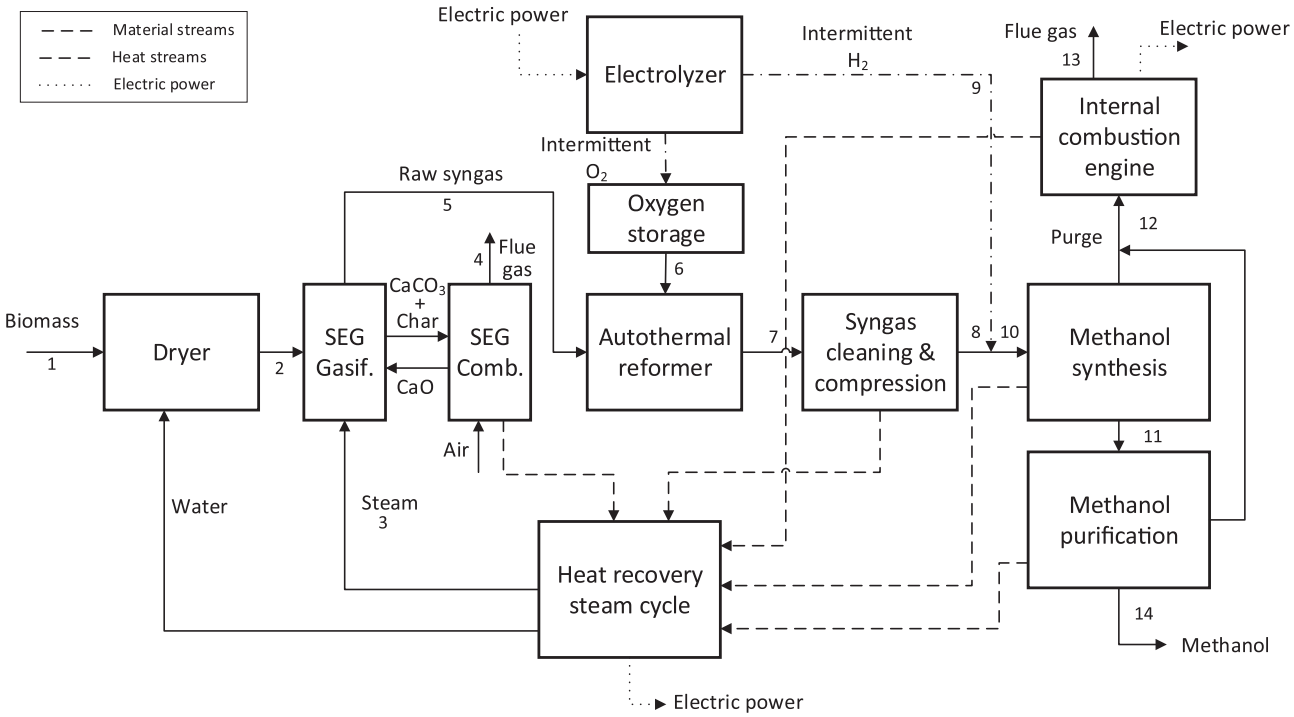

Fig. 1. Block diagram of the assessed Power & Biomass-to-Methanol plant.

is fed to the ATR to reach the exit temperature of 800 °C. An oxygen storage is foreseen in order to store the intermittent oxygen production from the electrolyzer. Methane conversion through the ATR is assumed to be 90%.

The reformed syngas (stream 7) is then fed to the cleaning section which includes the removal of undesirable compounds, such as sulfur, chlorine and alkali, that would poison the downstream catalytic reactor. The cleaning section includes a water scrubber, H_2S absorption by liquid Redox LO-CAT process [16] and adsorption with activated carbon. Before the activated carbon unit, syngas is compressed to 90 bar. When hydrogen from electrolysis is available (stream 9), it is compressed from 30 to 90 bar and mixed with syngas upstream the methanol synthesis section to obtain a syngas with the proper 'M' module of 2.05 (stream 10).

A conventional methanol synthesis technology is adopted, based on a boiling water reactor (BWR) where the syngas flows through tubes filled with catalyst and surrounded by boiling water at 238 °C. Since the per-pass methanol yield is limited by thermodynamic equilibrium, most of the unconverted reactants are recycled back to the reactor. The crude methanol is cooled down to 40 °C, separated from the light gases in a flash unit and then throttled to about 2 bar before purification. The purification section includes distillation columns aimed at stripping off the light gases from the crude methanol and at separating water from the methanol, to reach the target purity of 99.85%$_{wt}$.

The purge from the methanol synthesis and purification units (stream 12) contains a significant amount of light gases, whose heating value is exploited in a cogenerative internal combustion engine for electricity and steam production. A steam cycle is included in the plant in order to recover the heat from the different sections and to produce electricity and steam for internal consumption.

The plant unit operations must be designed to manage the intermittent addition of hydrogen, since the electrolyzer is turned on only when the electricity price allows an economically viable hydrogen production. Therefore, two main operating points are assessed, namely (i) baseline operation (i.e. without hydrogen addition) and (ii) enhanced operation (i.e. with hydrogen addition).

The process model is developed in Aspen Plus®, which allows to compute the mass and energy balances of the integrated plant. The computations are conducted for a biomass input of 100 MW_{LHV}. The proximate and the ultimate analysis of the as-received biomass are assumed from literature [17] and are reported in Appendix.

For the thermodynamic properties, different models are considered for the different plant sections, to improve the accuracy of calculations for the different processes. The general model is the RKS-BM that is complemented with the SRK model in the methanol synthesis section, the NRTL model in the methanol purification section and the ELECNRTL model in the water scrubber.

A description of the plant units and of the methods for the simulation is given in the next sections. An extensive table with the main calculation assumptions is reported in the Appendix (Table A1).

2.1. *Biomass pre-treatment*

Biomass pretreatment [18,19] includes a belt drier. Heated air flows through the biomass bed, providing the heat for water evaporation. Hot water is used to heat the drying air by means of a heat exchanger. Air is blown through a thin static layer of material on a horizontally moving permeable belt.

The dryer is designed to provide a biomass with an outlet temperature of 80 °C and a moisture content of 15%$_{wt}$. The low-temperature belt dryer described in [20] is adopted in the process model. A hot water loop with temperatures ranging between 90 and 30 °C provides the necessary thermal power for the dryer, which has a specific heat demand of 1 MWh/t_{H2O} evaporated resulting in a duty of about 13 MW_{th}. The power consumption is set to 32 kWh/t of dry feedstock [4].

2.2. *Sorption-enhanced gasification (SEG)*

The SEG section includes the dual-fluidized bed system, constituted by a bubbling fluidized bed (BFB) gasifier/carbonator and a circulating fluidized bed (CFB) combustor/calciner. Low pressure steam is fed to the BFB reactor as gasifying agent to reach the target steam-to-carbon ratio (S/C) of 1.5. Additional steam and air are also consumed with sealing purposes in biomass feeder, solid purge and filter cleaning.

Table 2
ERD plant stream properties in baseline operation.

Stream #	1	2	3	4	5	6	7	8 = 10[1]	11	12	13	14
Stream description	As-received biomass	Dried biomass	Fluidizing steam	Flue gas from combustor	Raw syngas	Oxygen to reformer	Reformed syngas	Syngas to synthesis	Methanol to purification	Purge to ICE	Flue gas from ICE	Methanol
Temperature, °C	25.0	80.0	182.0	156.1	714.1	25.0	800.0	122.7	41.6	35.9	360.0	64.1
Pressure, bar	1.01	1.01	2.00	1.05	1.23	30.00	1.10	92.00	2.00	1.36	1.01	1.01
Mass flow rate, kg/s	10.27	6.64	4.70	16.97	8.68	0.54	9.22	4.37	4.12	0.33	2.71	3.12
Mole flow rate, kmol/h	–	–	939.7	1843.7	2059.4	61.26	2285.4	1318.1	543.2	78.25	356.3	350.3
Composition, $\%_{mol}$	–	–	–	–	–	–	–	–	–	–	–	–
H_2O	–	–	100	0.91	49.11	–	42.25	–	33.76	0.29	17.75	0.19
H_2	–	–	–	–	32.91	–	40.58	70.36	0.16	49.22	–	–
CO_2	–	–	–	27.89	7.12	–	8.35	14.39	0.82	8.05	4.98	–
CO	–	–	–	–	4.39	–	7.45	12.92	–	0.71	–	–
Methanol	–	–	–	–	–	–	–	–	64.88	2.46	–	99.78
CH_4	–	–	–	–	4.30	–	0.39	0.67	0.23	11.26	–	–
C_xH_y	–	–	–	–	1.08	–	–	–	–	–	–	–
O_2	–	–	–	2.99	–	100	–	–	–	–	5.98	–
Ar	–	–	–	0.85	–	–	–	–	–	–	0.81	–
N_2	–	–	–	67.36	1.07	–	0.96	1.67	0.13	27.97	70.49	–
Ethanol	–	–	–	–	–	–	–	–	0.02	–	–	0.03
DME	–	–	–	–	–	–	–	–	–	0.03	–	–
LHV, MJ/kg	9.74	16.37	–	–	9.28	–	8.42	17.76	15.25	14.94	–	19.90
Power, MW_{LHV}	100.0	108.76	–	–	80.56	–	77.68	77.65	62.86	4.94	–	62.00

[1] In baseline operation, stream 8 coincides with stream 10 and hydrogen addition (i.e. stream 9) is not present.

The gasifier is modelled with a 0D model. Following the method proposed in [21], the parameter $p_{\delta_{WGS}}$ is used to determine the approach to equilibrium of the water gas shift (WGS) reaction through eq. (2-1), where p_i is the partial pressure of the *i-th* species in the syngas and $K_p(T)$ is the WGS equilibrium constant from [22].

$$p_{\delta_{WGS}} = log_{10}\left[\frac{\Pi_i p_i^{\nu_i}}{K_p(T)}\right] \quad (2\text{-}1)$$

The methane content in the syngas is given as a methane production per unit of dried biomass fed to the gasifier. The content of higher hydrocarbons, lumped with the molecule C_2H_4, is given as molar production per unit of produced methane.

Char conversion in the gasifier depends on the gasification temperature, through the expression derived from the data in [22].

The uptake of carbon dioxide by CaO may be limited either by the chemical equilibrium or by the maximum conversion of CaO into $CaCO_3$. An approach to the equilibrium composition is considered, as indicated in [22]. The maximum conversion of CaO into $CaCO_3$ within the gasifier is calculated as function of the number of carbonation-calcination

Table 3
ERD plant stream properties in enhanced operation.

Stream #	1	2	3	4	5	6	7	8	9	10	11	12	13	14
Stream description	As-received biomass	Dried biomass	Fluidizing steam	Flue gas from combustor	Raw syngas	Oxygen to reformer	Reformed syngas	Syngas before enriching	Hydrogen	Syngas to synthesis	Methanol to purification	Purge to ICE	Flue gas from ICE	Methanol
Temperature, °C	25.0	80.0	400.0	143.9	771.8	25.0	800.0	120.5	25.0	118.5	40.9	32.5	360.0	64.1
Pressure, bar	1.01	1.01	1.96	1.05	1.23	30.00	1.10	92.00	30.00	92.00	2.00	1.36	1.01	1.01
Mass flow rate, kg/s	10.27	6.64	4.44	14.01	10.86	0.44	11.30	6.63	0.37	6.99	6.67	0.53	4.57	4.97
Mole flow rate, kmol/h	–	–	887.5	1615.2	2190.6	50.05	2404.0	1472.8	654.1	2126.9	875.3	143.6	603.4	559.1
Composition, $\%_{mol}$	–	–	–	–	–	–	–	–	–	–	–	–	–	–
H_2O	–	–	100	3.81	44.41	–	38.64	–	–	–	33.69	0.41	19.80	0.15
H_2	–	–	–	–	28.41	–	35.72	58.31	100	71.13	0.21	62.45	–	–
CO_2	–	–	–	17.76	13.19	–	13.13	21.31	–	14.75	1.52	13.28	5.44	–
CO	–	–	–	–	8.25	–	11.28	18.41	–	12.75	0.01	1.06	–	–
Methanol	–	–	–	–	–	–	–	–	–	–	64.35	2.57	–	99.81
CH_4	–	–	–	–	3.82	–	0.35	0.57	–	0.39	0.13	5.81	–	–
C_xH_y	–	–	–	–	0.96	–	–	–	–	–	–	–	–	–
O_2	–	–	–	3.00	–	100	–	–	–	–	–	–	6.02	–
Ar	–	–	–	0.93	–	–	–	–	–	–	–	–	0.81	–
N_2	–	–	–	74.50	0.95	–	0.86	1.41	–	0.98	0.07	14.39	67.93	–
Ethanol	–	–	–	–	–	–	–	–	–	–	0.03	–	–	0.05
DME	–	–	–	–	–	–	–	–	–	–	–	0.02	–	–
LHV, MJ/kg	9.74	16.37	–	–	7.59	–	7.16	12.20	119.96	17.85	15.05	16.38	0.00	19.91
Power, MW_{LHV}	100.0	108.76	–	–	82.39	–	80.89	80.86	43.94	124.80	100.32	8.67	0.00	99.01

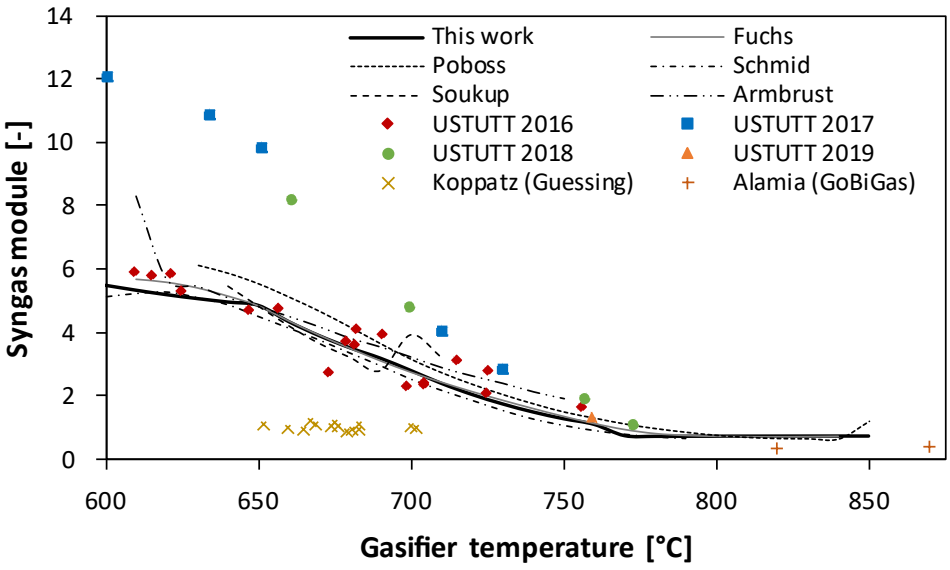

Fig. 2. Syngas module as a function of the gasifier temperature from the 0D model of this work, compared with the data from literature [22,25–30] and with experimental campaigns conducted in the FLEDGED H2020 project framework at the University of Stuttgart (USTUTT) [31–34].

cycles, according to [23]. In order to take account of kinetics limitation, the residence time and the distribution of the particles in the gasifier, a ratio between actual and maximum conversion of 0.75 is assumed for the sorbent. However, for all the investigated cases, CO_2 uptake resulted to be controlled by the thermodynamic limitation (i.e. by the CO_2 partial pressure) and to be never limited by the availability of active CaO in the circulating sorbent.

The content of other species in the syngas is estimated by assuming that all the sulfur in biomass is converted to H_2S, all chlorine to HCl and 10% of the nitrogen to NH_3.

Being the gasifier a BFB, the model considers an almost complete separation of solids from gas. The solids entrained by gases out of the cyclones are assumed to be 0.01% of the circulating solids.

The recirculated solids are fed to the combustor which performs the complete combustion of the unconverted char and of the additional biomass needed to achieve the target combustor temperature of 910 °C. In the combustor, complete calcination of calcium carbonate is achieved.

Since the combustor is a CFB, the solids are assumed to be entrained by the gas with a certain solid mass flow per cross-section unit (G_S) at raiser outlet, by following the approach in [24]. The outlet section of the combustor is designed to have a gas velocity of 5 m/s. The relation between entrained solids flow rate $\dot{m}_{es}$, G_S and gas velocity is given by eq. (2-2), where $\dot{m}_{gas}$ is gas mass flow rate, ρ_{gas} is gas density and v_{gas} the assumed gas velocity.

$$\dot{m}_{es} = G_S \bullet \frac{\dot{m}_{gas}}{\rho_{gas} \bullet v_{gas}} \tag{2-2}$$

The solids are separated by the outlet cyclone with a given efficiency which is specified to be 99.9% for calcium and 99% for ashes in order to take account of the different particle size distribution. The separated solids are partly sent to the gasifier and partly recirculated to the CFB combustor riser. A minimum solid purge from the bottom bed is required to avoid alkali and ashes collection in the reactor, therefore a mass flow rate equal to 1% of the inlet biomass is removed from the combustor. A makeup of limestone is added to the combustor to compensate the solids lost in the purge and from the cyclones. Combustion air is preheated by flue gases up to 270 °C in design operation. The air flow rate is adjusted to obtain 3%$_{mol}$ of oxygen concentration in the flue gases.

The connection between dual-fluidized bed system requires equal pressures in the two beds. Since the gasifier is operated above the atmospheric pressure to keep the whole syngas cooling and cleaning line at positive pressure, the combustor is also kept at pressure (~1.4 bar) through a backpressure valve before the stack.

The flexible operation of the sorption-enhanced gasification unit involves the production of syngas with a module close to 2 in baseline operation and lower than 1 in enhanced operation. The module is controlled by increasing the sorbent circulation rate which causes an increase of the gasification temperature from 714 °C in baseline operation to 772 °C in enhanced operation. The latter condition leads to zero CO_2 absorption in the gasifier due to thermodynamic limitation. In this way, the syngas retains the maximum amount of carbon (i.e. all the carbon except the unconverted char in the gasifier), which determines the maximum amount of hydrogen addition. Therefore, in enhanced operation the circulating CaO has the only function of heat carrier in the indirect gasification loop. Fig. 2 compares the dependency of the syngas module on the gasifier temperature obtained with the 0D model in this work against experimental and modelling data in the literature.

Table 4 provides the details of the SEG reactor in the baseline and enhanced operating conditions. The char conversion is higher in enhanced operation, due to higher temperature gasification. This requires part of the input biomass to be fed to the combustor in order to achieve the target temperature. As a result of the mass and energy balances, the carbon efficiency of the SEG unit (i.e. the ratio between the carbon in the syngas stream and the inlet biogenic carbon) increases from 42.7 to 68.7% from baseline to enhanced operation. On the other hand, the increase of fuel efficiency (referred to the dried biomass) is relatively small, from 74.08 to 75.76%.

The combustor is designed in baseline operation, due to the higher flue gases flow rate resulting from the higher combustion power needed for sorbent calcination and from the released CO_2. In enhanced operation, the solid flux at the combustor riser outlet G_s decreases from 30 to 25.4 kg/m^2 s due to the lower mass flow rate and the lower gas density. At the same time, the solids circulation rate between the combustor and the gasifier increases from about 39 kg/s to 137 kg/s, as heat is transferred to the gasifier under a lower temperature variation of the circulating solids. This increased solids circulation corresponds to a minimum flux in the riser of 19.5 kg/m^2 s, which is lower than the actual solids flux, demonstrating that solids circulation can be sustained by the fluid-dynamics of the CFB combustor.

Fig. 3 shows the energy balance of the SEG section in baseline and in enhanced operation, respectively on the left and on the right. The inner

Table 4
SEG operating conditions and exit gas composition in baseline and enhanced operations.

Parameter	Baseline operation	Enhanced operation
Gasifier exit temperature, °C	714.1[1]	771.8[2]
H_2, $\%mol_{dry}$, N_2, Ar free	66.08	52.01
CO, $\%mol_{dry}$, N_2, Ar free	8.82	15.11
CO_2, $\%mol_{dry}$, N_2, Ar free	14.30	24.14
CH_4, $\%mol_{dry}$, N_2, Ar free	8.64	6.99
C_xHy, $\%mol_{dry}$, N_2, Ar free	2.16	1.75
H_2O, %mol	49.12	44.42
Syngas module at gasifier outlet	2.24	0.71
Syngas flow rate, kmol/h	2059	2191
Char conversion in the gasifier, % of inlet C	68.06	72.81
Absorbed CO_2, % of inlet C	25.31	0.00
Biomass to gasifier, % of inlet biomass	100.0	94.34
Carbon efficiency, % of inlet C	42.71	68.69
Fuel efficiency, $\%_{LHV}$ of dried biomass	74.08	75.76
Flow rate of solids from combustor to gasifier, kg/s	39.29	137.16
CaO conversion in the gasifier, %	8.95	0.00
Gas superficial velocity at combustor outlet, m/s	5.00	4.38
Solid flux at combustor riser outlet (G_s), kg/m^2 s	30.01	25.44
Minimum solids flux to ensure the solids circulation, kg/m^2 s	5.58	19.48

[1] Gasification temperature is tuned to have a module equal to 2.05 upstream the methanol synthesis.
[2] Gasification temperature is tuned to have no absorbed CO_2 in the gasifier.

circle refers to the input energy to the SEG, the outer refers to the output energy.

The largest part of the input energy is associated to the chemical energy of biomass. Minor contributions derive from the sensible heat of the other streams fed to the SEG unit. In the enhanced operation, the sensible heat contribution associated with the input steam to the gasifier is twice as high the one in baseline operation. This is due to the fact that in enhanced operation the steam is fed to the gasifier at a higher temperature (400 °C) than in baseline operation (182 °C), which allows to decrease the additional biomass input required by the combustor. However, in baseline operation there is no need of additional biomass to the combustor and a higher steam input temperature would require combustor cooling or higher flue gas temperature.

In both the operating modes, about 72% of the energy output is represented by the chemical energy (LHV basis) of the raw syngas exiting the process. However, less than 49% is useful chemical energy associated to CO and H_2, which can be converted in the downstream synthesis process. More than 23% of the SEG output energy is associated to the heating value of methane and higher hydrocarbons which cannot be exploited for methanol production. This is the reason why a reforming unit downstream the gasification island is needed to achieve competitive performance of the overall plant. Significant contributions to the outlet energy flow are related to the sensible heat of the syngas exiting the gasifier and to the combustor flue gases. The higher contribution to the flue gas cooler for the baseline operation is due to the additional quantity of CO_2 released by sorbent calcination.

2.3. Syngas purification, conditioning and compression

Downstream the gasification unit, the raw syngas undergoes a high temperature filtration at the gasifier outlet temperature and is then fed to the raw gas reformer. The reforming unit is an ATR fed with oxygen produced as a by-product from the water electrolysis, using catalysts designed to operate on raw syngas [35]. A restricted equilibrium calculation approach has been adopted for the ATR, assuming 90% methane conversion and complete conversion of higher hydrocarbons. The assumed methane conversion is slightly higher than the conversion achieved in VTT lab-scale pilot plant [36]. An oxygen storage is associated with the reforming unit in order to store the intermittent oxygen production from the electrolysis and to provide a stable flow to the ATR. The minimum capacity factor of the electrolyzer which is required to produce the needed oxygen without external import or back-up ASU is 18.6%. By assuming 3 h of back-up time, an oxygen storage size of about 149 m^3 is needed for storing gaseous oxygen at around 30 bar and ambient temperature. Information about the operating conditions of the ATR are reported in Table 5. The higher oxygen demand to heat up the raw syngas to the reforming temperature of the baseline operation is due to the lower gasifier exit temperature.

Downstream the ATR, syngas is cooled down to 220 °C and scrubbed with water. The scrubber inlet temperature is chosen to avoid the condensation of residual tars [37]. Ammonia and chlorine contained in the gas are removed in the scrubber.

Bulk sulfur removal is performed through a liquid Redox unit (LO-

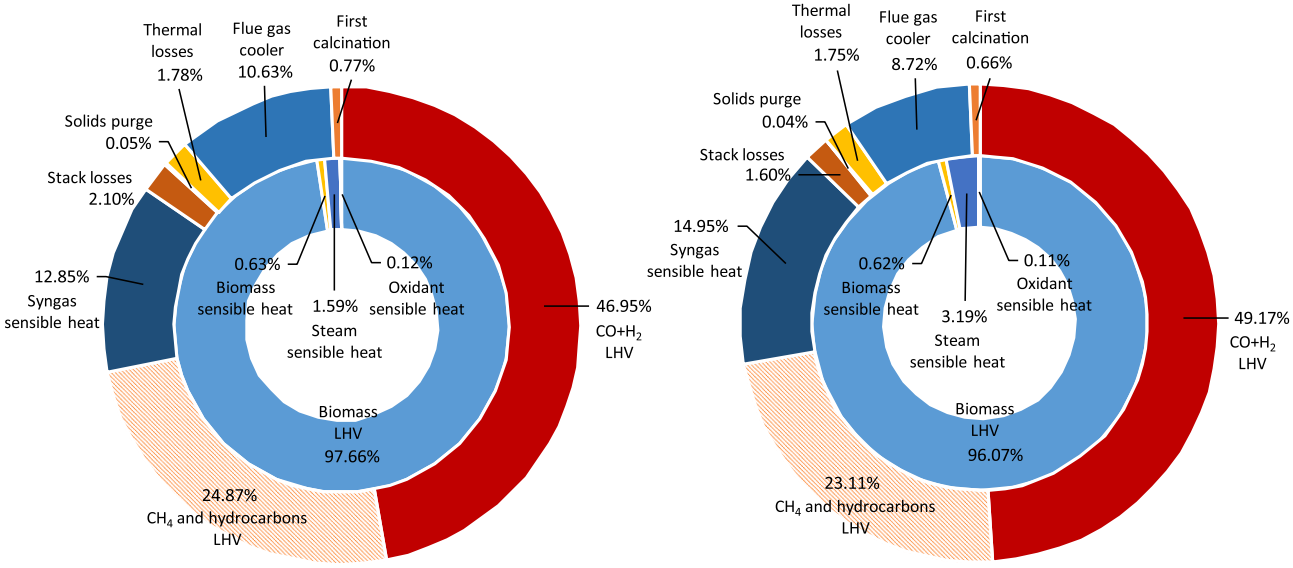

Fig. 3. Energy balance of the SEG process. The inner circle refers to the input energy, the outer refers to the output energy. Left: baseline operation. Right: enhanced operation.

Table 5
Autothermal reformer operating conditions and exit gas composition in baseline and enhanced operations.

Parameter	Baseline operation	Enhanced operation
Oxygen input, kmol/h	61.26	50.05
H_2, $\%mol_{dry}$, N_2, Ar free	71.46	59.05
CO_2, $\%mol_{dry}$ N_2, Ar free	14.71	21.71
CO, $\%mol_{dry}$ N_2, Ar free	13.12	18.64
S/C at reformer inlet	2.73	1.63
Syngas module at reformer exit	2.04	0.93

CAT process), where H_2S is converted into elemental sulfur and water by reaction with an iron oxygen carrier. The system is simulated as a black box, with data from [38].

After bulk cleaning, syngas is compressed in a 7-stage intercooled compressor, with an outlet pressure of about 90 bar and intercoolers outlet temperature of 40 °C. Pressure ratio per stage β_{stage} is about 1.9, leading to gas temperature at the outlet of each compression stage 125 °C. In enhanced operation, the volumetric flow rate at the syngas compressor inlet increases by 11.7% compared to the baseline operation. This variation can be managed and it is assumed not to affect the compression efficiency.

Activated carbon bed and sulfur scavenging units, used to remove trace contaminants that may poison the catalyst, are placed upstream the last compression stage at a pressure of about 48.6 bar.

The H_2 enrichment step in the enhanced operation mode is realized just upstream the methanol synthesis section. The water electrolysis unit is designed to provide the maximum hydrogen enrichment in order to retain all the carbon in the syngas. This results in a 63.3 MW_{el} electrolyzer which provides 0.37 kg/s of pure hydrogen at 30 bar, that is further compressed to about 90 bar by a 2-stage intercooled compressor without aftercooler before mixing with the syngas stream.

2.4. Methanol synthesis

Once purified, conditioned and compressed, the fresh syngas is fed to the methanol synthesis island. The syngas specifications in both the operating modes are shown in Table 6. The composition of the fresh syngas shows limited variation in the baseline and in the enhanced operating modes. This also applies to the CO/CO_2 ratio and it largely results from the chemical equilibrium of the WGS reaction at the ATR outlet. The major difference between the baseline and enhanced operation cases lies in the flow rate, which is about 60% higher in the enhanced operation compared to the baseline.

The fresh syngas is first mixed with the unconverted recycled gas and then preheated in a feed/effluent heat exchanger, upstream the methanol synthesis reactor. The temperature of the inlet syngas to the methanol synthesis reactor is set according to the heat exchanger specifications. The outlet crude methanol is cooled down until the dew point temperature of the mixture is reached. The crude methanol is further cooled down to 40 °C and separated in a flash unit from the light gases which are recycled back to the reactor.

The methanol synthesis reactor is a multi-tubular fixed-bed reactor, externally cooled by boiling water and filled with cylindrical pellets of a commercial methanol synthesis catalyst $Cu/ZnO/Al_2O_3$ (CZA). The behavior of the reactor is simulated with a 2D + 1D mathematical model, considering a heterogeneous model of a single tube. The model consists of i-species mass and energy 2D balances for the gas phase, accounting for axial and radial concentration and temperature gradients, coupled with gas–solid continuity equations and 1D i-species mass balance in isothermal cylindrical pellets, in order to properly account for the intra-particle diffusion limitations. The model includes also a 1D momentum balance to evaluate the pressure drops along the reactor tubes. The physico-chemical properties of the gas mixture are calculated with the gPROMS® utility tool Multiflash, while the mass and energy transport correlations and the friction factor are taken from literature references. The well-established kinetic model of Vanden Bussche et al. [39] for the methanol synthesis is used in the simulations. The model is described in detail in the literature work of Montebelli et al. [40]. The axial coordinate is discretized using a first-order backward finite-difference method (BFDM), while a third-order orthogonal collocation on finite elements method (OCFEM) is used for the radial and the pellet coordinates. On the basis of a convergence analysis, 60 discretization points are used along the axial coordinate in a non-uniform grid obtained by a logarithm transformation implemented in gPROMS® with a transformation parameter $\alpha = 15$, while, respectively, 3 and 4 collocation elements are used for the tube radial coordinate and for the catalyst pellet coordinate. The differential–algebraic equation system is implemented in gPROMS® software for the numerical solution.

The methanol synthesis process and reactor design are based on the evaluation of the performance, reported in terms of carbon yield and methanol productivity, and on the analysis of the catalyst temperature which must be controlled in order to prevent excessive temperature hot-spot that may lead to catalyst deactivation by Cu cluster sintering [41].

The flexibility requirement also affects the methanol synthesis BWR, for which two different designs are proposed. The two alternatives entail different number of tubes and therefore different amounts of catalyst, selected either to keep high methanol yield in the enhanced operating mode (enhanced reactor design or ERD) or to limit the reactor investment costs (baseline reactor design or BRD). Both the ERD and BRD configurations have some fixed design criteria, among which are the tube length and diameter (i. e. 6 m and 0.04 m, respectively), the reactor pressure and the temperature of the boiling water (i.e. 90 bar and 238 °C, respectively).

The number of tubes inside the reactor for each configuration depends on the selected gas hourly space velocity (GHSV), referred to the volume of the reactor tubes. The ERD configuration is designed with a GHSV of 5000 h^{-1} in enhanced operation with a recycle ratio (RR, defined as the molar flow rate of the recycle stream divided by the molar flow rate of the fresh syngas) of 5. In the baseline operation mode, the recycled molar flow rate is kept constant, fixed by the blower design, which involves an increase of RR. In this way, in the baseline operating mode the decrease of GHSV is limited and the overall methanol yield is maximized. The BRD configuration is designed with a GHSV of 5000 h^{-1} and with a RR of 5.0 in the baseline operating mode. When hydrogen is injected into the process, the recycled molar flow rate is kept constant, fixed by the blower design, and the RR reduces. In this way, a limited increase of the GHSV and a decrease of the overall methanol yield is obtained. Indeed, the yield performance is reversely correlated to the GHSV: high space velocity leads to lower methanol yield as consequence of the short gas/catalyst contact time (Table 7). Thus, the BRD solution is characterized by a lower methanol yield with respect to the ERD, but it guarantees savings on the reactor investment since less reactor tubes are employed. Furthermore, the BRD configuration shows an overall productivity which is higher with respect to the ERD. Differently to the yield, the productivity is indeed favored by large GHSV.

The performance of the methanol synthesis reactor are reported in Table 7. The methanol yield is computed as follows, where F_i are the molar flow rates of the –i molecule.

Table 6
Syngas specifications upstream the methanol synthesis island in baseline and enhanced operating conditions.

Parameter	Baseline operation	Enhanced operation
Temperature, °C	122.7	118.5
Pressure, bar	92.0	92.0
Mass flow rate, kg/s	4.37	6.99
Molar flow rate, kmol/h	1318.1	2126.9
H_2, $\%mol_{dry}$, N_2, Ar free	71.55	71.83
CO_2, $\%mol_{dry}$, N_2, Ar free	14.63	14.90
CO, $\%mol_{dry}$, N_2, Ar free	13.14	12.87
CH_4, $\%mol_{dry}$, N_2, Ar free	0.68	0.40
CO/CO_2	0.90	0.86

Table 7
Performance of methanol synthesis reactor for both ERD and BRD configurations.

Parameters	ERD, baseline operation	ERD, enhanced operation	BRD, baseline operation	BRD, enhanced operation
Number of tubes	7580	7580	4704	4704
GHSV, h^{-1}	4684	5000	5000	5512
RR, molar basis	8.06	5.00	5.00	3.10
Recycle flow rate, kmol/h	10625	10625	6595	6595
Methanol yield per pass, %	48.61	46.50	43.07	37.23
Equilibrium yield per pass, %	62.14	64.31	57.92	55.82
Overall methanol yield, %	97.93	96.29	95.40	89.10
Syngas module at reactor inlet	8.60	6.84	5.71	3.98
Inert (CH_4, N_2) concentration at reactor inlet, $\%_{mol}$	37.25	18.71	25.00	8.20
Syngas temperature at reactor inlet, °C	183.3	172.3	175.1	167.8
Thermal power released by the reactor, MW	1.95	5.05	3.20	6.26
Methanol concentration at reactor outlet, $\%_{mol}$	3.56	5.22	5.15	7.14
Methanol concentration at flash unit outlet, $\%_{mol}$	64.88	64.35	64.75	64.30
Methanol productivity, $kg/day/kg_{cat}$	7.10	11.35	11.15	16.91

$$Yield = \frac{F_{M,out} - F_{M,in}}{(F_{CO_2} + F_{CO})_{in}} \quad (2\text{-}3)$$

The inert concentration at the reactor inlet is directly related to the RR which is adopted in the specific operating mode. The thermal power released by the reactor reduces if the content of inerts increases.

The molar fraction of the reactants (H_2, CO_2 and CO) and products (H_2O and methanol) is higher in the enhanced operating modes. Conversely, the amount of inert gases (N_2 and CH_4) is far larger in the baseline operations (in particular in ERD where it approaches ~ 40%), coherently with the higher inert concentration in the inlet streams. However, the methanol yield per passage is lower in the cases with H_2 addition in absolute value and also if compared with the equilibrium one. This is due to the larger production of water that inhibits the reaction kinetics.

An important parameter to consider in the analysis is the maximum catalyst temperature. The hot-spot temperature should be limited, to avoid the CZA catalyst deactivation due to the Cu clusters sintering [41]. The calculated catalyst centerline temperature axial profiles are reported in Fig. 4. In all cases analyzed, the temperature increases in the inlet zone of the reactor, driven by the heat provided by the boiling water (238 °C). The heat released by the exothermic reactions makes the temperature increase to a hot-spot maximum (reached between 1 and 2 m for all the case analyzed) and then the temperature flattens at the boiling water value due to the decrease of reaction rates related to the approach to the thermodynamic equilibrium. The parameter that mainly controls the temperature in the four cases analyzed is the amount of inerts ($N_2 + CH_4$) at the reactor inlet. Indeed, the smoothest temperature profile with the lowest hot-spot (245 °C) is obtained in the ERD baseline operating mode, due to dilution effect given by the largest amount of inerts that is ~ 37% in molar fraction. Instead, the highest hot-spot (252 °C) is obtained in the BRD enhanced operating mode where the inerts are only ~ 8%. The other two cases, ERD enhanced operating mode and BRD baseline operating mode, have ~ 19% and ~ 25% of inert gas content respectively and show the same intermediate hot-spot temperature (248 °C). The differences are however minimal due to the relatively low exothermicity of the methanol synthesis from CO_2 (ΔH_r = -49.4 kJ/mol_{CO2}) and since the effect of the lower inerts concentration is partly compensated by the higher GHSV (i.e. higher flow velocity) and the larger thermal conductivity (related to the high conductivity of the molecular hydrogen) in the enhanced operations. All in all, the maximum temperature are well below the critical temperature limit of 300 °C reported in literature for the catalyst CZA catalyst [41]. Therefore, the reactor can manage efficiently the thermal duty in each of the cases analyzed.

2.5. Methanol purification

Upstream the methanol purification island, the raw methanol is expanded to 2 bar by means of a valve and reaches a temperature of about 40 °C. The raw product is composed of methanol (~64%$_{mol}$), water (~33%$_{mol}$) and other components (mainly low boiling impurities and traces of ethanol), with a different composition for each considered case, as reported in Table 8. In the enhanced operation mode, the flowrate of methanol to be purified increases by 62% for the ERD case and by 55% for the BRD case with respect to baseline operation. Such

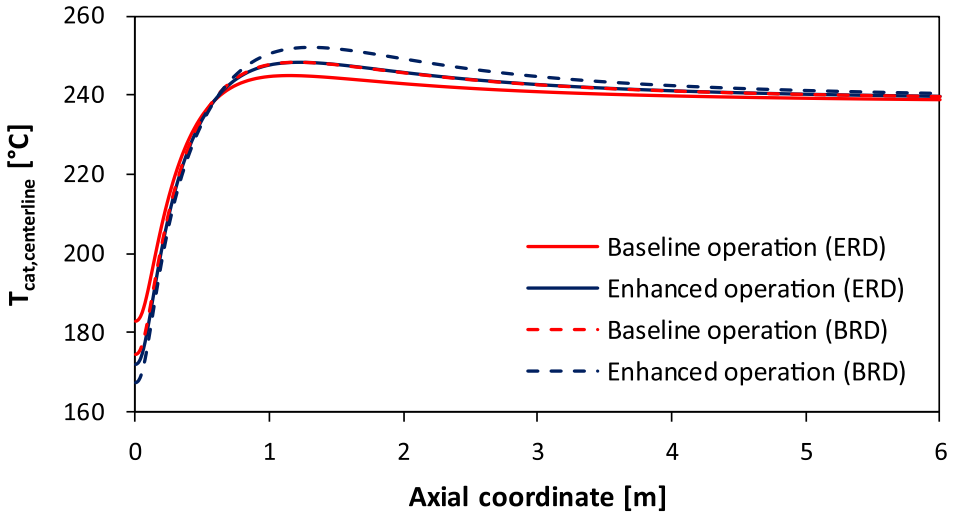

Fig. 4. Catalyst centerline temperature axial profiles.

Table 8
Characteristics of the raw methanol streams fed to the purification section for the assessed cases.

Parameter	ERD, baseline operation	ERD, enhanced operation	BRD, baseline operation	BRD, enhanced operation
Mass flow rate at purification inlet, kg/s	4.12	6.67	4.06	6.28
Molar flow rate at purification inlet, kmol/h	543.22	875.27	530.38	810.07
Methanol concentration at purification inlet, $\%_{mol}$	64.88	64.35	64.75	64.30
H_2O concentration at purification inlet, $\%_{mol}$	33.76	33.69	33.03	31.78
Stabilizing column				
Condenser duty, MW	0.011	0.023	0.016	0.043
Reflux ratio	0.10	0.10	0.10	0.10
Reboiler duty, MW	0.66	1.08	0.66	1.04
Boilup ratio	0.13	0.13	0.13	0.14
Concentration column				
Condenser duty, MW	6.31	10.17	6.18	9.49
Reflux ratio	0.85	0.87	0.86	0.88
Reboiler duty, MW	6.24	10.06	6.11	9.39
Boilup ratio	3.01	3.01	3.09	3.23

flow rate variation must be managed by the purification unit.

The purification section is composed, for all the cases, of two distillation trayed columns in series. The first unit is a stabilizing column operating at 1.3 bar, aiming at removing the low boiling impurities. The heavier stabilized methanol-rich stream is fed to the second column, a concentration column run at atmospheric pressure, to obtain the methanol product stream with a purity of 99.85%$_{wt}$. The recovery in this stream of the methanol fed to the purification section is greater than 99%. The two columns are simulated with a rate-based approach, to take into account the mass transfer occurring on each tray.

The first column performs the separation with 23 valve trays and the second one with 48 valve trays. The selected diameter allows to operate the columns in the two operating modes without significant issues of flooding or weeping, which would decrease the separation performance of the column. To this aim, for both the stabilizing unit and the concentration one, the dimensions are determined on the basis of the highest feed flowrate, resulting in diameters of 0.7 m for the stabilizing column and $\sim$ 2 m for concentration column.

In all the cases, the reflux ratio and the boilup ratio for the stabilizing column are low, in the range of 0.10–0.14, because of the low vapor being condensed at the top and because of the low amount of liquid being vaporized in the reboiler. As for the concentration column, which performs the separation between the two main components, higher amounts of circulating flowrates are needed, which involves high reflux and boilup ratios.

2.6. Heat recovery and power generation

Cooling of the SEG process streams and methanol synthesis reactors make available a large amount of heat which needs to be efficiently recovered. Additional waste heat is generated by the internal combustion engine (ICE) which uses the off-gas of the methanol synthesis and purification units. The performance map of the ICE as a function of its size S and load L are assessed using the linearized equation (2-4) derived in [42]:

$$P = k_1 L + k_2 S + k_3 \tag{2-4}$$

where L is the load as thermal input power, S is the ICE size and k_1, k_2 and k_3 parameters obtained in [42] by best-fitting the part-load maps of commercially available gas-fired ICEs with power output larger than 4 MW. Variations of the exhaust temperature with loads have been neglected.

In total, the waste heat made available in the temperature range 1000 °C to 30 °C ranges from 79 MW for the enhanced operating mode to 66 MW for the baseline mode. Such power figures fall in the size range typical of heat recovery steam cycles (HRSCs) which could be used to efficiently convert into electrical power the excess heat. On the other hand, the heat-related data depend on the operating mode calling for a flexible design of the heat exchanger network (HEN) and HRSC. For this reason, multiperiod methodologies must be used to find the optimal arrangement of the HEN and HRSC.

In this work, the multiperiod synthesis methodology recently proposed in [43,44] has been adopted. Compared to previously developed approaches, it allows optimizing the design of the HEN and HRSC in an integrated manner while considering all the key technical design constraints, the different operating modes of the plants and the trade-off between operating and investment costs.

The superstructures used here for the integrated synthesis of HEN and Rankine cycles are those proposed by [45] and used in the subsequent improvements [46,47]. It is an extension of the well-known SYNHEAT stage-wise HEN superstructure proposed by [48] in which utility and Rankine cycle streams are included as hot/cold flows with variable mass flowrates.

The scheme of the *p-h* superstructure considered for the HRSC is shown in Fig. 5. The cycle features up to 3 evaporation pressure levels (120 bar, 32 bar, 6.5 bar), 3 condensation levels (6.5 bar, 2 bar, 0.05 bar), extractions of superheated steam for the process, and a deaerator. The evaporation pressure levels and the condensation pressure levels have been set on the basis of the process requirements of reaction steam and reactor cooling:

- The medium-pressure level (MP) evaporation temperature is fixed by the MeOH reactor temperature (238 °C, corresponding to an evaporation pressure of 32.2 bar).
- The low-pressure level (LP) evaporation and condensation pressure is fixed at 6.5 bar.
- High-pressure evaporation level (HP) is set at 120 bar with a superheat temperature of 525 °C with the aim of avoiding using too expensive high grade steels for the superheater tubes; the reheater temperature is set to 480 °C in order to have the very LP (LLP, corresponding to 2 bar) steam turbine extraction at the temperature required by the gasifier (182 °C).
- Since the gasifier requires in the enhanced operating mode superheated steam at low pressure and high temperature (400 °C), a very low pressure reheater is included in the superstructure. It is worth noting that Fig. 5 shows the most general HRSC superstructure and, since the synthesis methodology optimizes also the installation of the evaporation and condensation levels, the optimal solution might be a simpler HRSC configuration (where some evaporation levels or condensation levels are not installed).

The multi-period design problem is formulated as a non-convex MINLP problem. Two types of variables are defined: operational variables for each period (namely, mass flowrates of utility streams, heat exchanged in each heat exchanger, charge state of the energy storage and temperatures of the streams entering/exiting the heat exchangers), and design variables for the selection of the installed units and the

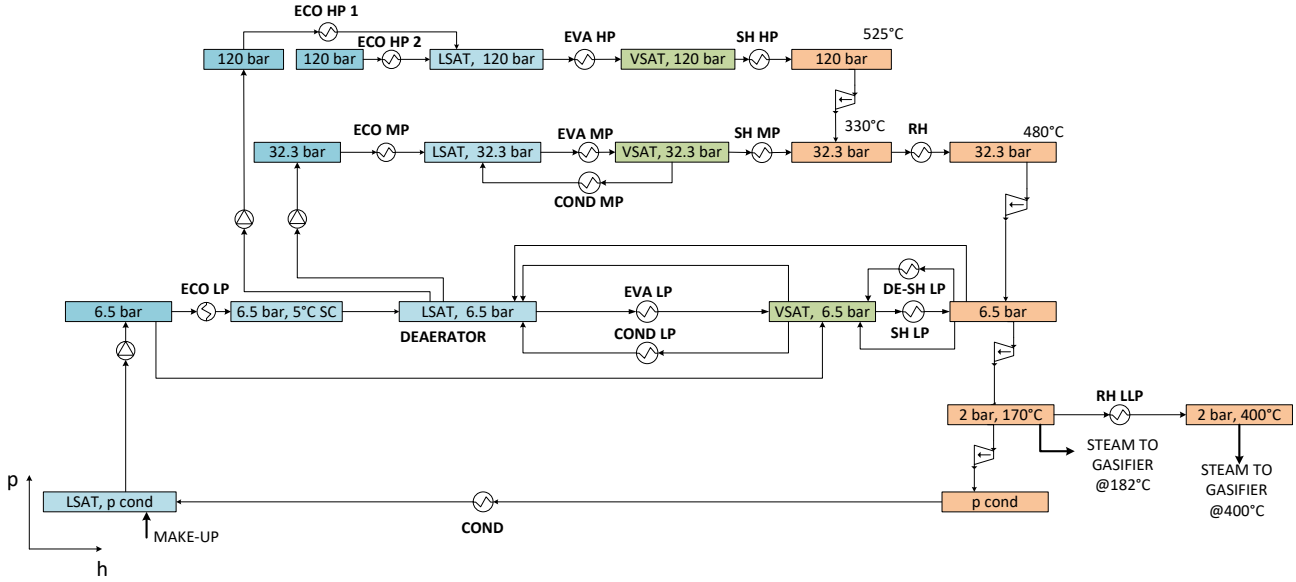

Fig. 5. Scheme of the p-h superstructure representing the possible HRSC configurations. Colored boxes denote steam/water headers at fixed pressures and temperatures, which are connected by equipment units (pumps, economizers, evaporators, superheaters, valves), as described in [46].

optimization of their sizes (namely, binary installation variables and sizes for the components of the Rankine cycle, for the heat exchangers and for the other utility systems). The objective function is the total annual cost of the heat recovery system (HEN and HRSC) of the plant, consisting in the sum of the annualized investment cost and the operating costs (revenues obtained from electricity sales are considered as negative operational costs). Similar to design problem of the HRSC for the LBJ plant [49], the problem constraints include forced matches (i.e., the methanol reactor must generate medium pressure steam), forbidden matches (i.e., to avoid metal dusting in the syngas cooler tubes) as well as the no-stream splitting constraint for the syngas stream. The problem has been solved using the decomposition algorithm specifically devised in [43,44].

In Table 9, the ICE and the heat recovery steam cycle electric power outputs and net electric efficiencies are shown for the different cases, with the reference BtM plant included. The highest electricity production from the ICE for the BRD enhanced operation is related to the lowest RR in the methanol synthesis unit and therefore to the highest purge flow rate. The same reasoning can be extended to the baseline ERD, which shows the lowest ICE electricity production due to the highest RR and the consequent lowest purge flow rate. As mentioned above, the net electric efficiency of the ICE decreases in baseline operation according with the decrease of the thermal power of the purge flow from the methanol synthesis and purification island. The ICE in the BtM plant displays higher electric power output and efficiency than ICE in the baseline operating modes because it operates in design condition.

As far as the HRSC design and performance are concerned, the optimal design substantially depends on the availability of high temperature heat and on the required steam exports of the different cases/operating modes. Due to the lower high temperature heat available in the ERD plant and the higher methanol production, leading to higher heat demand for methanol purification, the optimal HRSC results to be without the HP evaporation level, differently from the BRD and the reference plants. As a result, also the efficiency and power output are significantly lower in the ERD plant.

In Figs. A1 and A2, the complete temperature heat diagram and the grand composite curve of the PBtM plant with ERD design in enhanced operation mode are reported.

3. Process simulation results

To evaluate the performance of the assessed Power & Biomass-to-Methanol plant, the following key performance indicators have been used.

The *fuel efficiency* ($\eta_{F,i}$) is the ratio between the chemical energy of the product stream and the chemical energy input to the process (both based on LHV). The fuel efficiency can be evaluated for the whole plant or for any plant process unit (i). In the enhanced operation mode, the

Table 9
ICE and heat recovery steam cycle electric power outputs and net electric efficiencies. Steam flow rates at HP (120 bar), MP (32.2 bar) and LP (6.5 bar) turbine inlet are also reported.

Parameter	ERD, baseline operation	ERD, enhanced operation	BRD, baseline operation	BRD, enhanced operation	Reference BtM plant
ICE					
Electric power, MW	2.15	4.00	2.73	7.91	3.17
Net electric efficiency, %	43.23	46.40	39.96	46.40	46.40
HRSC					
HP/MP evaporation pressure levels, bar	32.2		120/32.2		120/32.2
Steam flow rate at HP turbine inlet, kg/s	–	–	8.1	7.5	8.5
Steam flow rate at MP turbine inlet, kg/s	7.4	4.5	9.6	10.3	9.5
Steam flow rate at LP turbine inlet, kg/s	7.2	6.1	9.3	9.9	9.2
Net electric power, MW	4.24	2.95	8.30	8.02	8.02
Net electric efficiency, %	20.52	14.76	29.31	28.54	30.38

energy input includes also the contribution of the inlet hydrogen.

$$\eta_{F,i} = \frac{\dot{m}_{out,i} \bullet LHV_{out,i}}{\dot{m}_{in,i} \bullet LHV_{in,i}} \tag{3-1}$$

The *useful fuel efficiency* ($\eta^{u}_{F,i}$) accounts for the useful reactants (j) and the useful products (k) of the single plant unit (e.g. biomass as reactant and H_2 and CO as products for the gasification section, H_2 and CO as reactants and methanol as product for the methanol synthesis section).

$$\eta^{u}_{F,i} = \frac{\sum_{j=1}^{N} \dot{m}_{out,i,j} \bullet LHV_{out,i,j}}{\sum_{k=1}^{M} \dot{m}_{in,i,k} \bullet LHV_{in,i,k}} \tag{3-2}$$

The *carbon efficiency* (CE_i) can be defined as the ratio between the carbon molar flow rate in the stream $F_{C,i}$ at the exit of each process unit i and the carbon molar flow rate in the inlet biomass stream $F_{C,biom}$.

$$CE_i = \frac{F_{C,i}}{F_{C,biom}} \tag{3-3}$$

The achievable CE of a biofuel production plant is usually limited by the lack of hydrogen and the excess of oxygen in the feedstock, compared to the C:H:O ratio of the final product. The *potential carbon efficiency (PCE$_i$)* proposed by Poluzzi et al. [50] is also used, to track the effect on the achievable CE of processes that entail not only carbon separation, but also involve oxygen, water or hydrogen addition. For the production of a generic fuel $C_{\chi_C} H_{\chi_H} O_{\chi_O}$, the *PCE* is defined as the ratio between the maximum carbon flow rate in the final fuel obtainable from stream i and the total carbon flow rate in the inlet biomass (eq.(3–4)). The maximum fuel production $F_{fuel,max,i}$ is defined to take into account the potential loss of carbon and hydrogen associated to the removal of the excess oxygen.

$$PCE_i = \frac{F_{fuel,max,i} \bullet \chi_C}{F_{C,biom}} \tag{3-4}$$

A *useful potential carbon efficiency (PCE$^{u}_i$)* can also be defined, considering only the useful molecules for the synthesis of the specific fuel. In this case, inert compounds in the fuel synthesis process (e.g. methane in the syngas for the synthesis of methanol) do not contribute in the calculation of the efficiency.

The *electric efficiency* (*EE*) indicates the conversion of the biomass chemical energy into electricity. The net electric output (P_{el}) accounts for the electricity produced by the steam turbines and by the internal combustion engine and for the electric consumption of the auxiliaries.

$$EE = \frac{P_{el}}{\dot{m}_{biom} \bullet LHV_{biom}} \tag{3-5}$$

The *equivalent fuel efficiency* ($\eta_{F,eq}$) accounts for the biomass saving associated with the electricity production of the plant. A steam cycle with 35% of electric efficiency ($\eta_{el,ref}$) is assumed as a reference, considering a biomass-fed subcritical steam power plant.

$$\eta_{F,eq} = \frac{\dot{m}_M \bullet LHV_M}{\dot{m}_{biom} \bullet LHV_{biom} - \frac{P_{el}}{\eta_{el,ref}}} \tag{3-6}$$

To account for the e-fuel production efficiency, the *power-to-fuel efficiency* (η_{PtF}) of eq.(3–7) is used, where the numerator is the additional fuel production in enhanced operation (EO) with respect to the baseline operation (BO) and P_{el} represents the net electric power output of the plant in enhanced operation and in baseline operation. Therefore, P_{el} includes the electricity production by the HRSC and the ICE and the electricity consumption by the auxiliaries. In enhanced operation, it also includes the electricity consumption by the electrolyzer, for which an electricity to hydrogen LHV efficiency of 69% is assumed [51,52].

$$\eta_{PtF} = \frac{\left(\dot{m}_M \bullet LHV_M\right)_{EO} - \left(\dot{m}_M \bullet LHV_M\right)_{BO}}{P_{el,EO} - P_{el,BO}} \tag{3-7}$$

In order to avoid the dependency on the efficiency of the electrolysis system, a *hydrogen-to-fuel efficiency* (η_{HtF}) is also used by considering the marginal contribution of hydrogen injection in fuel production (eq. (3-8)).

$$\eta_{HtF} = \frac{\left(\dot{m}_M \bullet LHV_M\right)_{EO} - \left(\dot{m}_M \bullet LHV_M\right)_{BO}}{\dot{m}_{H_2} \bullet LHV_{H_2}} \tag{3-8}$$

The performance indexes of the assessed PBtM plants and of the reference BtM plant are reported in Table 10.

As mentioned above, the enhanced operation guarantees a higher utilization of the biogenic carbon contained in the feedstock compared to the baseline operation. The higher carbon utilization ensures a higher fuel efficiency and a higher useful fuel efficiency of the SEG unit.

The lower gasifier exit temperature and the higher methane content also cause a lower fuel efficiency of the reformer in baseline operation, due to the higher oxygen demand to heat up the raw syngas to the reforming temperature and to provide the heat for methane reforming. On the other hand, the gain in the useful fuel efficiency is higher in these cases, thanks to the higher amount of reformed CH_4.

As regards the methanol synthesis island, the higher yield of the baseline operation for both ERD and BRD configurations involves higher fuel efficiencies with respect to the enhanced operations. The difference of methanol yield and fuel efficiency between the baseline and the enhanced operations is relatively small for the ERD case, where methanol synthesis efficiency reduces by about 1 percentage point. On the other hand, in the BRD the fuel efficiency drops by about 5 points when operated in enhanced operation mode.

In the purification island, the BRD configuration in enhanced operation mode shows a slightly higher fuel efficiency and useful fuel efficiency due to the lowest content of water in the raw methanol feed.

The resulting fuel efficiency of the overall plant is higher in enhanced operation than in baseline operation for both ERD and BRD configurations. The ERD configuration is more fuel efficient than the BRD because of a more efficient methanol synthesis section. The fuel efficiency is 68.8% vs. 63.8% in enhanced operation for ERD and BRD cases respectively and 62.0% vs. 60.4% in baseline operation. The gap in global fuel efficiency between the two operating modes is lower in BRD configuration because the enhanced operation shows the lowest fuel efficiency of the methanol synthesis section (74.3%). The increase of carbon efficiency made possible by hydrogen addition is significant, especially with the ERD design, where it increases from 40.3% in baseline operation to 64.4% in enhanced operation mode.

The effect of hydrogen injection in boosting methanol production is higher in the ERD configuration than BRD and involves higher hydrogen-to-fuel (84.2% vs. 71.4%) and power-to-fuel efficiencies (57.5% vs. 52.3%).

The overall electric consumption in enhanced operation is dominated by the electrolysis consumption. The higher syngas mass flow rate and the inlet hydrogen also contribute in increasing the electric consumption for gas compression. The higher amount of waste water in the enhanced operating mode is due to the higher water flow rate produced as bottom product in the concentration column.

The technical performance of the reference BtM plant is identical to the BRD baseline operation as far as biomass conversion is concerned. However, since the oxygen is provided by a cryogenic ASU, there is an additional electric consumption, computed assuming a specific consumption of 0.272 kWh_{el}/kg_{O2} [53].

In Fig. 6, the trend of the carbon efficiency, potential carbon efficiency and useful potential carbon efficiency is reported for the baseline and for the enhanced operating mode of the ERD configuration. The trend of the carbon efficiency indexes is qualitatively the same in the BRD plants, which are not shown. The evolution of all these indicators is followed along intermediate streams within the plant by following the approach adopted in Poluzzi et al. [50]. In the bar chart, the total

Table 10
Overall performance of Power & Biomass-to-Methanol plants.

Performance indexes	ERD, baseline operation	ERD, enhanced operation	BRD, baseline operation	BRD, enhanced operation	Reference BtM plant
$\eta_{F,dry}$, %	108.75	108.75	108.75	108.75	108.75
$\eta_{F,SEG}$, %	74.08	75.76	74.08	75.76	74.08
$\eta^{u}_{F,SEG}$ (input: biomass; output: H_2, CO), %	48.40	51.51	48.40	51.51	48.40
$\eta_{F,ref}$, %	96.42	98.18	96.42	98.18	96.42
$\eta^{u}_{F,ref}$ (input and output: H_2, CO), %	143.78	141.03	143.78	141.03	143.78
$\eta_{F,pur}$, %	99.96	99.96	99.96	99.96	99.96
$\eta^{u}_{F,pur}$ (input and output: H_2, CO), %	100.00	99.99	100.00	99.99	100.00
$\eta_{F,MeOH\_syn}$, %	80.95	80.39	78.83	74.30	78.83
$\eta^{u}_{F,MeOH\_syn}$ (input: H_2, CO; output MeOH), %	82.56	81.22	80.44	75.12	80.44
$\eta_{F,MeOH\_pur}$, %	98.63	98.69	98.63	98.97	98.63
$\eta^{u}_{F,MeOH\_pur}$ (input and output: MeOH), %	99.24	99.16	99.17	99.37	99.17
$\eta_{F,global}$,%	62.00	68.78	60.37	63.75	60.37
$\eta_{F,eq}$, %	57.19	33.25	64.20	33.90	63.47
Carbon efficiency, %	40.34	64.40	39.27	59.67	39.27
Oxygen demand in the reformer, kg/s	0.54	0.44	0.54	0.44	0.54
Methanol production, kg/s	3.12	4.97	3.03	4.61	3.03
Methanol output, MW_{LHV}	62.00	99.01	60.37	91.76	60.37
Methanol yield, %	97.93	96.29	95.40	89.10	95.40
H_2 addition, kg/s	–	0.37	–	0.37	–
H_2 addition, MW_{LHV}	–	43.94	–	43.94	–
Methanol production enhancement, %	–	59.63	–	51.93	–
η_{PtF}, $MW_{LHV,M}/MW_{el}$	–	57.48	–	52.27	–
η_{HtF}, $MW_{LHV,M}/MW_{H2}$	–	84.21	–	71.44	–
Net electric output, P_{el}, MW	−2.86	−67.24	2.03	−58.01	1.66
Electric generation, MW	6.38	6.95	11.02	15.92	11.19
Electric consumption, MW	9.24	74.19	8.99	73.93	9.53
Belt dryer	0.65	0.65	0.65	0.65	0.65
SEG air fan	0.75	0.73	0.75	0.73	0.75
Syngas compressor	7.15	7.95	7.15	7.95	7.15
Hydrogen compressor	–	0.88	–	0.88	–
Recycle compressor	0.67	0.67	0.41	0.41	0.41
Electrolyzer	–	63.29	–	63.29	–
Other auxilieries[1]	0.03	0.03	0.03	0.03	0.03
ASU	–	–	–	–	0.53
Total waste water, kg/s	5.77	6.16	5.73	5.97	5.73

[1] Other auxiliaries include Liquid Redox and water scrubber pump.

amount of each atom is represented by the complete bar enclosed in the red contour. The yellow part of the bars represents the maximum amount of each atom that can end up in the final product, therefore, they are in the same proportion as the corresponding atoms in the final product. The blue part of the bars shows the potential loss of carbon and hydrogen to separate the excess oxygen as H_2O or CO_2. Oxygen excess is distributed to carbon and hydrogen in order to maximize the yield of final product. The red part of the bar (when present) represents the excess of hydrogen or carbon after the removal of the excess oxygen.

As-received biomass features a carbon-to-hydrogen ratio much higher than that of methanol (0.70 vs. 0.25) and the oxygen excess causes the PCE to be equal to 70%. By means of the drying process, part of the water is removed from the biomass and this results in a PCE decrease to about 47%. In the dried biomass, hydrogen becomes the limiting element, therefore the oxygen excess can be removed as CO_2 without affecting the maximum fuel yield, as excess carbon remains available (red portion of the C bar).

As shown in Fig. 6 (top) which describes the baseline operation, the PCE decreases to about 43% in the SEG unit. This is due to the loss of carbon from the gasifier to the combustor, where the char is burned and the absorbed CO_2 is vented. This represents the main loss of carbon, which is intrinsic in indirect gasification processes and is responsible for the lower carbon efficiencies achievable compared to systems based on direct gasification processes, as discussed in [50]. As a result of the carbon loss in the gasifier, carbon becomes the limiting element in the raw gas, that features a hydrogen excess (red portion of the bar). CE also drops in the gasifier to the same value of the PCE, due to carbon separation through both the unconverted char and the absorbed CO_2. Simultaneously, the PCE_u reduces to about 27% because of the presence of CH_4 and C_xH_y, which are inert in the downstream methanol synthesis. No substantial variation of the PCE occurs across the reformer for the assumed conditions, as the added oxygen can bond with the excess hydrogen and be entirely removed as water. On the other hand, the PCE_u increases to about 42% due to the conversion of the hydrocarbons into useful reactants (H_2 and CO). As the extent of CO_2 separation in the SEG is tuned to achieve the target syngas module after the reformer, no change of PCE and CE is observed in the conditioning step, which consists in a simple water separation. The final overall carbon efficiency in baseline operation is about 40.3% for the ERD configuration and about 39.3% for the BRD configuration. The slight difference between the two is mainly due to the different performance of the methanol synthesis section.

In enhanced operation, carbon separation is controlled by increasing the solid circulation rate and therefore the gasifier temperature compared to the baseline operation. The raw syngas features a higher CE compared to the baseline operation (about 69%), since less carbon is separated in the gasifier. The PCE of the raw syngas in enhanced operation is about 6% higher than baseline operation thanks to a higher content of carbon, which was the limiting element in the baseline operating mode. The PCE reduces within the reformer from about 49% to 45%. Then, CE and PCE do not change through the cleaning and conditioning step. The gap between the CE and the PCE represents the gain of carbon efficiency that may be achieved by hydrogen addition. This gap is filled in the enriching stage, where the PCE increases to the

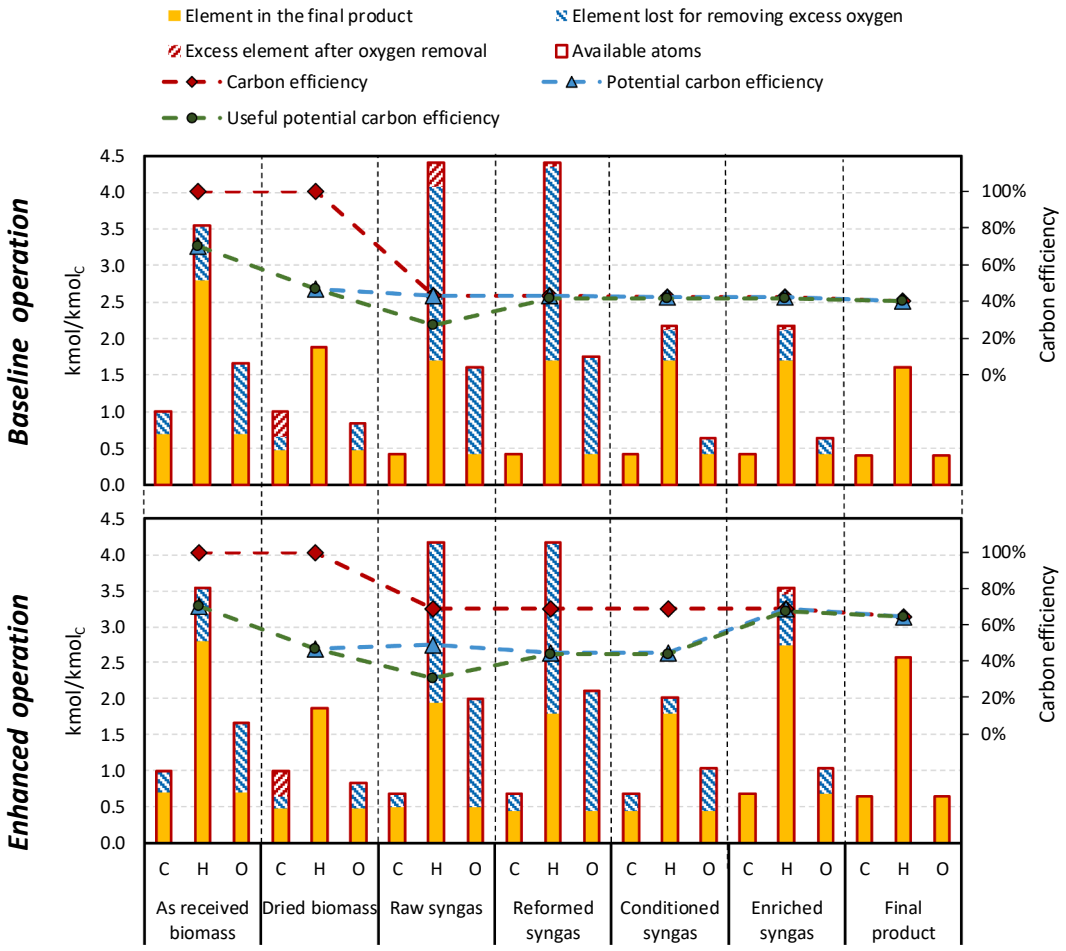

Fig. 6. Carbon efficiency, potential carbon efficiency and useful potential carbon efficiency of the process in baseline (top) and enhanced (bottom) operation for the ERD configuration.

same value of the CE. As shown in the bar chart, the added hydrogen allows to recover the carbon which is potentially lost to remove the excess oxygen, behaving as an oxygen acceptor. The final overall carbon efficiency in enhanced operation is about 64.4% for the ERD configuration and about 59.7% for the BRD configuration. The difference between the two is mainly due to the different performance of the methanol synthesis section, which is amplified compared to the baseline operation cases.

4. Economic analysis

4.1. Levelized cost of electro-fuel

The method applied for the economic analysis of the PBtM plants is the *Levelized Cost* approach. As discussed further on, a differential economic analysis approach is adopted, with the aim of quantifying the economic impact of the electrolysis integration in the assessed biofuel production plants. The levelized cost of the fuel is defined as the breakeven selling price that at the end of the plant lifetime (LT) repays the total cost (C_{tot}) by producing a certain amount of fuel (M_{tot}). It considers the total capital investment costs (*TCI*), utilities costs (C_{ut}), cost of feedstock ($C_{feedstock}$) and the fixed O&M costs ($C_{fixedO\&M}$), as shown in eq.(4–1), where $\dot{m}_{fuel}$ is the nominal fuel production rate and h_{eq} are the equivalent yearly operating hours, defined as the ratio between the actual amount of fuel produced in a certain period and the nominal flow rate.

$$LCOF = \frac{C_{tot}}{M_{tot}} = \frac{TCI \bullet CCF + C_{fixedO\&M} + C_{feedstock} + C_{ut}}{\dot{m}_{fuel} \bullet h_{eq}} \tag{4-1}$$

The flexible PBtM plants operate in the two different modes: baseline operation (without hydrogen injection) and enhanced operation (with hydrogen injection). Since in the two cases both productivity and operational costs are different, they have to be weighted in order to calculate how they contribute to the total cost. In the analysis, the final LCOF is calculated by weighting the production and the operational costs on the hours for the two operation modes, according to eq. (4-2), where χ_{BO} and χ_{EO} are the fraction of total operating hours in baseline and enhanced mode respectively, and h is the annual plant availability.

$$LCOF = \frac{C_{tot}}{M_{tot}} = \frac{TCI \bullet CCF + C_{fixedO\&M} + C_{feedstock} + (C_{ut,BO} \bullet \chi_{BO} + C_{ut,EO} \bullet \chi_{EO})}{(\dot{m}_{fuel,BO} \bullet \chi_{BO} + \dot{m}_{fuel,EO} \bullet \chi_{EO}) \bullet h} \tag{4-2}$$

The Capex estimation approach is based on the *Percentage of Delivered-Equipment Cost Method*, which requires the determination of the delivered-equipment cost for estimating the fixed-capital investment (FCI), the working capital (WC) and the total capital investment (TCI). The other items included in the TCI computation are then estimated as percentage of the delivered-equipment cost. This is summarized in the following cost equations:

$$FCI_i = E_i \cdot \left(1 + \sum_j^M f_j\right) \tag{4-3}$$

$$WC_i = f_{WC} \cdot E_i \tag{4-4}$$

$$TCI = \sum_i^N (FCI_i + WC_i) \tag{4-5}$$

The FCI of the *i*-th plant component is estimated with the equation (4–3) where E_i is the delivered-equipment cost of the *i*-th component and f_j are the *M* multiplying factors reported in Appendix B (Table B1). The delivered equipment costs are mostly derived from authors' database, with the exception of the ASU (taken from [54]) and of the power island (where the cost functions in [49] have been used). The working capital is computed with the equation (4–4), where f_{WC} is one of the multiplying factors of the delivered-equipment cost reported in Appendix B (Table B1). Finally, the TCI is computed as the summation over the total number of components *N* of the FCI_i and WC_i. All the costs reported in this work refer to the year 2019.

To take into account the investment depreciation and the change in the value of money, a Capital Charge Factor can be introduced, representing the fraction of TCI assigned to each year of operation during its lifetime LT.

$$CCF = \frac{1}{\sum_{LT} \frac{1}{(1+\alpha)^n}} = \frac{\alpha(1+\alpha)^{LT}}{(1+\alpha)^{LT} - 1} \tag{4-6}$$

The discount rate α is a lumped parameter considering depreciation rate, inflation, expected return on investment (equity) and interests on capital of debt. The last contributions are sometimes labeled as WACC (Weighted Average Capital Cost).

In order to compute the Opex, the following costs are determined: utilities, maintenance and repairs, operating supplies, operating labor, laboratory costs, local taxes, insurance, catalyst.

The main costs of the utilities are for the feedstock and for the electricity. Because of the differential economic analysis approach and the fixed biomass flow rate fed to all the plants, the results of this work are independent of the biomass feedstock cost, which is therefore not reported. As regards the cost of electricity, the 2019 electricity prices of the day-ahead market of West Denmark (DK1) are considered in the calculations [55]. Denmark has been selected as it is the European country with the highest share of intermittent renewable energy sources and therefore may be representative of the energy mix of other European countries in the coming decade. The average electricity price can be derived as a function of the operating hours from the cumulative electricity price duration curve. Therefore, once the electrolyzer capacity factor is fixed (80% in this analysis, as reference value), an average electricity price of 34.3 €/MWh in enhanced operation and 55.3 €/MWh in baseline operation can be computed. It has to be noted that the environmental and economic impacts of indirect CO_2 emissions associated to the electricity consumed by the electrolyzer are not accounted in this study. In other words, it is assumed that zero-emissions electricity is consumed by the electrolyzer (which is not the case of the average power generation plant in the current Denmark energy mix). The use of near zero-emission electricity is a pre-requisite in the production of hydrogen from electrolysis and of related e-products, to make them environmentally sustainable and with lower carbon footprint than conventional products [56].

As regards the catalyst cost, according to [57], a typical price for the commercial CZA methanol catalyst is 18.12 €/kg with a catalyst lifetime of 4 years.

The maintenance and repairs include the cost of maintenance labor and materials, including equipment spares, needed for the maintenance of the plant. The annual maintenance cost is taken as 5% of the fixed capital cost. The cost can be considered to be divided evenly between labor and materials. The operating supplies refer to all the miscellaneous materials required to operate the plant, which are not included neither in the raw materials nor in the maintenance materials and have been assumed equal to 10% of the total maintenance cost. The operating labor is the manpower needed to operate the plant and it is directly involved with running the process. The costs should be calculated from an estimate of the number of shift and day personnel needed. Assuming highly automated plants, the operating labor has been assumed 10% of the total operating costs. As regards the laboratory costs, a value of 25% of the operating labor cost is assumed. For the local taxes and insurance, 1% of the fixed capital is considered for each.

Table 11
Main parameters for the economic analysis.

Economic parameters	Value
Discount rate, %	10
Lifetime, y	20
Capital Charge Factor, %	11.75
Annual availability, h/year	7884
Electrolyzer capacity factor, %	80
Denmark average electricity price, €/MWh	38.49
Denmark average electricity price, €/MWh (enhanced operation)	34.30
Denmark average electricity price, €/MWh (baseline operation)	55.26

A summary of the aforementioned key parameters which are used in the analysis is reported in Table 11 and in Appendix B (Table B2).

In this work, the aforementioned *Levelized cost* approach is applied in a differential way. The costs of the PBtM plants are compared with the costs of a BtM plant, whose main differences are the absence of the electrolysis system and the presence of an ASU to produce oxygen for the reformer. The objective of the differential approach is to evaluate if flexible PBtM plants are economically competitive with the reference BtM plant. In this regard, the Levelized Cost of the e-Fuel (LCOe-F) can be defined as in eq.(4–7), where ΔC_{tot} is the difference in total costs between PBtM and BtM plants, which results from the sum of the differential TCI and the differential $C_{O\&M}$, and $\dot{m}_{e\text{-}fuel}$ is the additional e-Methanol (e-MeOH) produced thanks to the electrolysis integration.

$$LCOe\text{-}F = \frac{\Delta C_{tot}}{e{-}M_{tot}} = \frac{\Delta TCI \bullet CCF + \Delta C_{fixedO\&M} + \Delta C_{ut}}{\dot{m}_{e\text{-}fuel} \bullet h_{eq}} \tag{4-7}$$

In Table 12, the fixed capital investment costs of the assessed plants are reported. Process units that do not differ in BtM and PBtM plants (e.g. biomass drying, gasifier and reformer) are not reported in the table as they do not affect the differential economic analysis. The PBtM plants benefit from the absence of the ASU, which is present in the BtM case. However, as already reported in Section 2.3, an oxygen storage is needed for the ATR. In this case, a 30 bar gaseous oxygen storage sized to cover 3 h of continuous operation is considered, whose costs was estimated to be

Table 12
Fixed capital investment costs of the units of the PBtM and the BtM plants used in the differential economic analysis. The units with the same investment cost in the different plants are not reported.

Fixed capital investment, M€	Reference BtM plant	BRD PBtM plant	ERD PBtM plant
Biomass-to-syngas island			
ASU (with O_2 compressor)	10.74	–	–
Oxygen storage	–	4.51	4.51
Cleaning and conditioning island			
Syngas compressor	19.88	21.35	21.35
Other units	6.72	6.94	6.98
Syngas-to-methanol island			
Methanol synthesis BWR	7.35	7.35	11.86
Recycle compressor	2.21	2.21	3.15
Stabilizing column	0.45	0.49	0.49
Concentration column	1.49	1.84	1.86
Power island			
CHP internal combustion engine	1.78	4.27	2.23
HRSC	33.43	40.45	26.13
Electricity-to-hydrogen island			
Electrolyzer	–	44.31	44.31
H_2 compressor	–	4.66	4.66
Total differential FCI	–	63.87	51.11

about 45% the avoided ASU cost. The capital investment for the syngas compressor is slightly higher for PBtM plants, since they are designed for a higher flow rate. The ERD option shows higher costs for both the methanol synthesis reactor and the recycle compressor, i.e. 11.9 M€ and 3.2 M€ respectively, compared to 7.4 M€ and 2.2 M€ of the BtM and BRD cases. As regards the two distillation columns, the PBtM plants display slightly higher capital investment, as both are designed for the enhanced operation. The advantage in capital cost of the BRD flexible plant, that benefits from a smaller methanol synthesis unit, is compensated by the higher cost of the power island, needed to recover the energy from the purge gas from the MeOH synthesis unit. Finally, the PBtM configurations exhibit a major additional cost for hydrogen production in the electrolysis unit and compression, which count for about 75–95% of the total differential FCI. The assumed specific cost for the electrolysis system is 700 €/kW_e which is consistent with the current alkaline technology and with the future cost estimations of PEM technology [52,56].

Overall, the cost of the larger steam cycle of the BRD plant with respect to the ERD plant, overcompensates the lower cost of the methanol synthesis island, resulting in higher differential FCI.

A degree of freedom in the plant design is the size of the oxygen storage. The optimal size depends on the frequency of electrolyzer switching. By assuming to store oxygen at the same production pressure of 30 bar and at 25 °C, the resulting density is 39.4 kg/m^3. With a reformer oxygen consumption in baseline operation of 0.54 kg/s, the volume of buffer storage for 3-hour operation without electrolysis is 149 m^3. An insufficient size of the storage may lead to the need of importing oxygen from an external producer or switching the electrolyzer on at low load to produce the exact amount of oxygen needed in the plant, when the electricity price is higher than the breakeven price.

When operated at full load, the oxygen produced by the electrolyzer is 4.4 times higher than the flow rate of oxygen required in the reformer (10.53 t/h vs. 1.96 t/h). Therefore, the minimum capacity factor of the electrolyzer to produce the oxygen required in the ATR without external import or back-up ASU is 18.6%. Possible revenues from the sale of the excess oxygen are not included in this analysis, although an economic income of about 2.9 M€ (about 20% of the annual electricity cost) may be obtained assuming an oxygen selling price of 54 €/t.

In Table 13, the main economic results of the levelized cost approach are shown. The ERD PBtM plant shows 1.5% higher differential total costs with respect to the BRD configuration, but ensures 24% higher e-Methanol production, leading to ~ 20% lower LCOe-F of the produced methanol. Although a consistent comparison with other studies is not possible, it is interesting to observe that the obtained LCOe-F costs lie in the upper range of the biomethanol costs obtained in the relevant literature reported in Table 1.

In Fig. 7, the LCOe-F breakdown is reported. The main contribution is associated to the purchase of electricity, whose share is about 48% and 56% in BRD and ERD plants, respectively. The share of the electrolyzer capital cost is about 20% in both cases. The fixed Opex share is in the range 22–24%, with BRD as upper bound. Other costs, resulting from the net contribution of the avoided ASU and the other capital investments, contribute by about 9% in BRD and 3% in ERD plants..

Overall, from this analysis, it can be concluded that designs aimed at high power-to-methanol conversion efficiencies (i.e. the ERD design in this case study) should be preferred due to the high cost of hydrogen production compared to the cost associated to oversizing the equipment for fuel synthesis.

Table 13
Main result of the economic analysis and levelized cost of e-fuel.

Economic results	BRD PBtM plant	ERD PBtM plant
Differential TCI, M€/y	7.50	6.00
Differencial fixed O&M, M€/y	6.50	5.99
Differential purchased electricity cost, M€/y	12.88	15.30
Differential total costs, M€/y	26.88	27.29
e-Methanol production, t/y	35,768	44,530
LCOe-F, €/t	751.4	612.9
LCOe-F, €/GJ	37.76	30.80

4.2. Sensitivity analysis

The LCOe-F is deeply influenced by the operating hours in enhanced operation and by the average electricity price. In Fig. 8, the dependency of the electrolyzer capacity factor and the average electricity price on the LCOe-F is shown for the ERD case. Increasing CF_{el} from 20 to 80%, leads to a reduction of the LCOe-F by about 30 €/GJ, independently of the average electricity price in enhanced operation.

The electrolyzer investment cost is also a key factor influencing the LCOe-F. Fig. 9 shows the effect of a reduction of the electrolyzer investment cost from 700 €/kW to 400 €/kW, considered as a potential cost in favorable long-term scenarios [58]. The benefit of a reduction of the cost of electrolysis is much higher for low capacity factors, where the costs of green hydrogen are dominated by the Capex. For CF_{el} of 20%, the LCOe-F cost reduces by 16.6 €/GJ with a low cost electrolyzer. For capacity factor of 80%, the LCOe-F reduction is 4.8 €/GJ, i.e. −15.6% than with the reference electricity price.

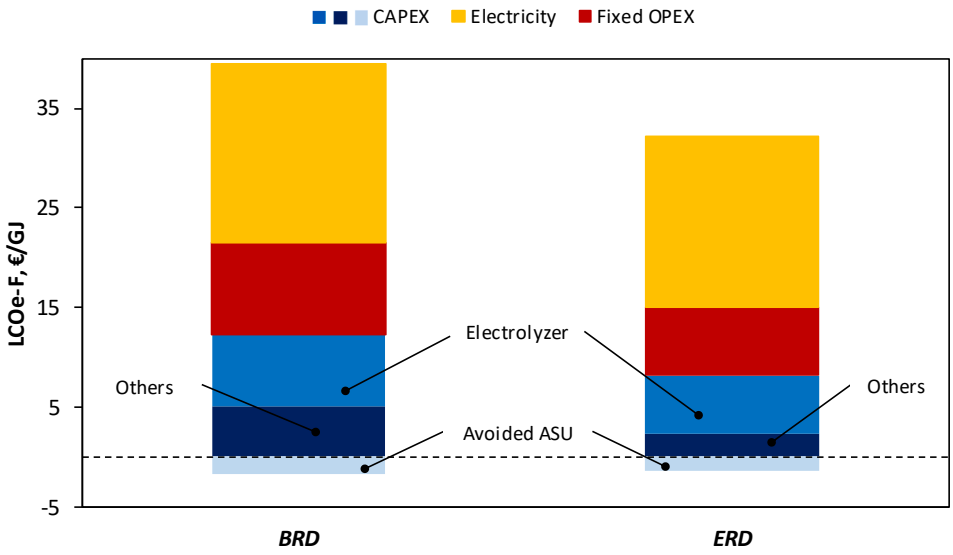

Fig. 7. LCOe-F breakdown for the BRD and ERD cases.

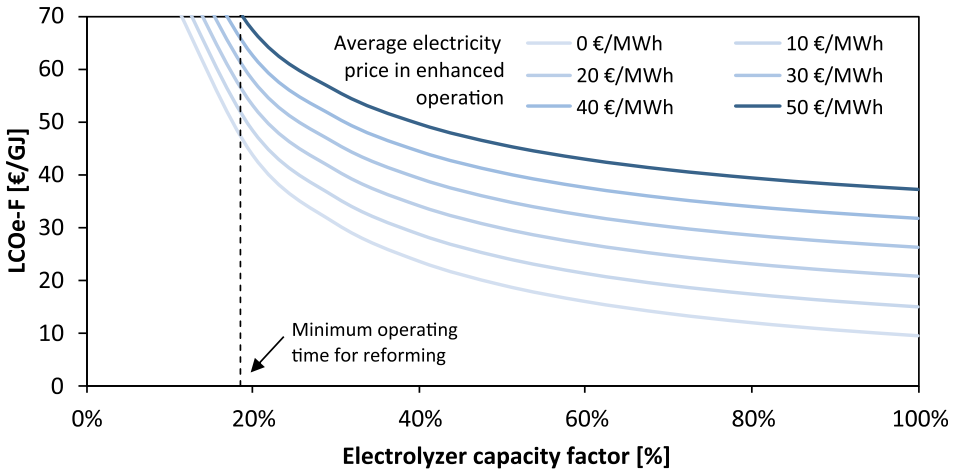

Fig. 8. LCOe-F of the ERD PBtM plant as a function of the electrolyzer capacity factor and of the average electricity price in enhanced operation, for an electrolyzer cost of 700 €/kW.

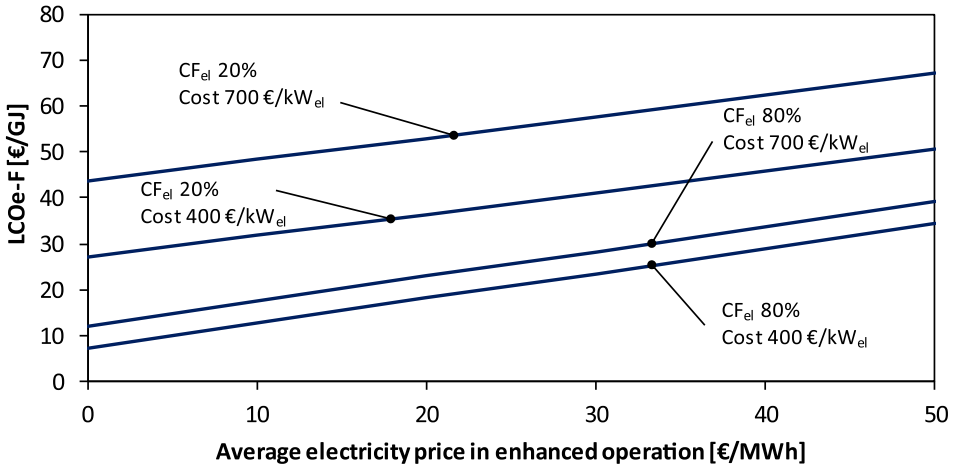

Fig. 9. LCOe-F for the ERD PBtM plant as a function of the average electricity price in enhanced operation. The different cases refer to changes in the electrolysis capacity factor (80% and 20%) and in the electrolysis investment costs (700 €/kW and 400 €/kW).

These results show that the impact of increasing the capacity factor from 20% to 80% on the cost of the e-fuel is significantly higher than the impact of a reduction of the electrolyzer capital cost, once the pre-requisite of high electrolyzer capacity factor is met.

4.3. Coupling with the electricity market

In order to evaluate the profitability of a flexible PBtM plant investment compared to a reference BtM plant or an inflexible PBtM plant, it is necessary to identify the number of hours of operation in baseline and enhanced operating modes and the corresponding electricity prices. The fraction of the total operating hours in baseline and enhanced operation can be estimated with the 'Willingness to Pay' (WTP) methodology [15].

The 'short-term WTP' is defined as the breakeven electricity price that makes economically profitable to switch on the electrolyzer and operate in enhanced mode. Under such conditions, the revenues from the additional methanol production compensate the additional operational costs (electricity and water). The short-term WTP (WTP_{ST}) can be calculated from eq. (4–8), where $\dot{m}_{fuel}$ is the fuel production in enhanced operation (EO) and baseline operation (BO), p_{fuel} is the fuel selling price (€/kg), P_{el} is the net electrical power purchased in EO and in BO and c_{water} is the cost of water (quantitatively negligible compared to the cost of electricity).

$$\left(\dot{m}_{fuel,EO} - \dot{m}_{fuel,BO}\right) \bullet p_{fuel} = WTP_{ST} \bullet \left(P_{el,EO} - P_{el,BO}\right) + c_{water} \quad (4\text{-}8)$$

Since all the contributions are proportional to the operational time, the result is independent of the capacity factor of the electrolysis unit. Taxes or grid fees are not accounted in this calculation. Moreover, the cost of water proves to be negligible compared to the cost of electricity.

The procedure is graphically illustrated in Fig. 10. The cumulative price duration curve (green) is generated by ranking all the hourly prices of the 2019 day-ahead market of West Denmark (DK1) in ascending order. A certain point of the curve indicates how long during the year the price has been equal or lower than a certain value. The ascending (red) and descending (blue) average price curves are obtained by averaging the values of the cumulative curve starting from the lowest price and from the highest price, respectively. So, the yearly average electricity price can be read on the right end of the red curve and on the left end of the blue curve. For example, if a methanol selling price of 450 €/t is assumed, a short term WTP of 46.5 €/MWh can be calculated from eq. (4–8). By comparing this value with the cumulative electricity price curve, the number of operating hours in enhanced operation can be estimated to be the 76.3%. For that electrolyzer capacity factor, the value on the ascending average electricity price curve identifies the average electricity price in enhanced operating mode (33.7 €/MWh in this example) and the value on the descending average electricity price curve identifies the average electricity price in baseline operating mode (53.9 €/MWh).

The electrolyzer capacity factor is deeply influenced by the shape of the cumulative electricity price duration curve which depends on different

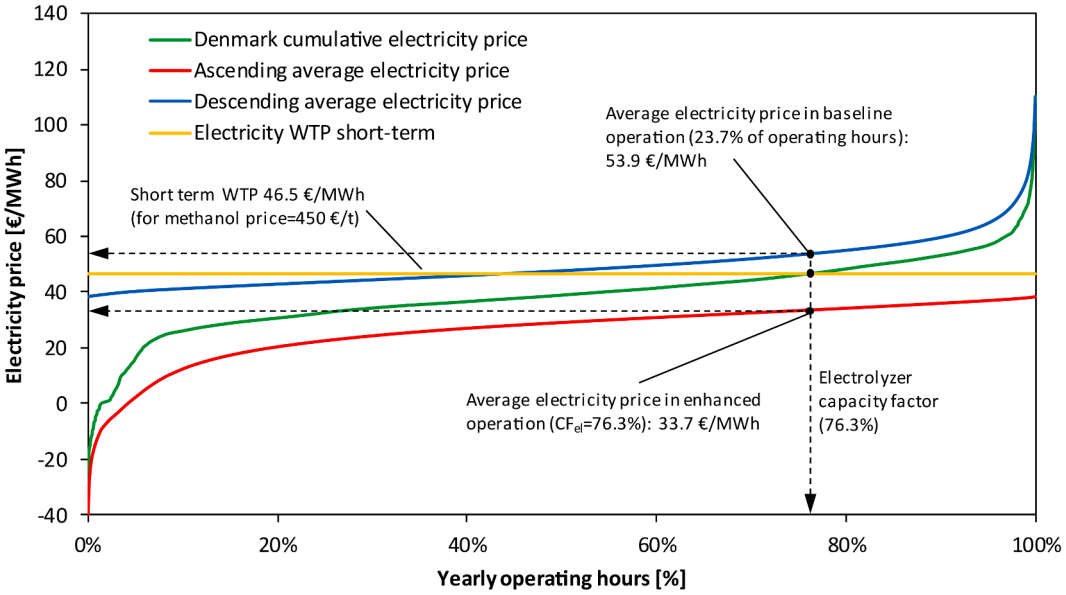

Fig. 10. Willingness to Pay approach with 2019 Denmark day-ahead market price curves. Breakeven points and resulting operating hours and electricity prices are shown for a methanol price of 450 €/t.

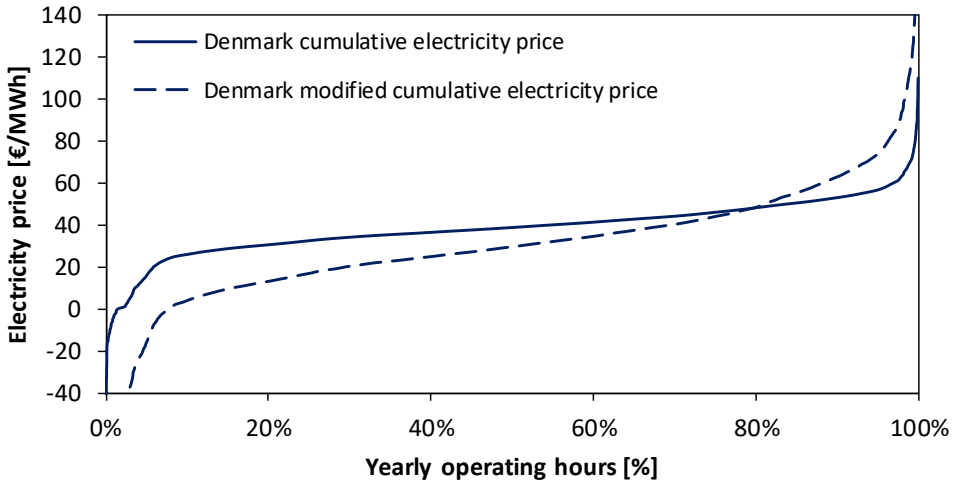

Fig. 11. 2019 Denmark cumulative electricity price and modified Denmark cumulative electricity price.

factors such as the location, the penetration of renewable energy sources (RES), the type of RES technology, the price of the fuel and the technology of fossil fuel power plants and the type of final user [59–62]. The general expected tendency is that by increasing the penetration of intermittent RES, the average electricity prices tend to reduce but the peak prices and the cost of grid balancing tend to increase. For the aforementioned reasons, a modified cumulative electricity price curve is added to the discussion, as shown in Fig. 11. It must be stressed that this hypothetical curve has no ambition of representing any specific future price curve. The aim here is to show the sensitivity of the results on a different curve shape featuring lower average electricity prices and amplified peak prices that may be reasonably expected in future electric systems.

Once the number of hours of operation in the two modes and the corresponding average electricity prices are identified for a certain methanol selling price, the profitability of the PBtM plant investment compared to the reference BtM option can be evaluated by computing the Net Present Value (NPV) and the Internal Rate of Return (IRR).

In Table 14, NPV and IRR are reported for two methanol selling prices, that lead to two different capacity factor of the electrolysis unit through the WTP methodology. The calculation is performed with two different capital investment of the electrolysis unit. A methanol selling price of 450 €/t (i.e. same order the market price of fossil methanol) involves an electrolysis capacity factor of 76.3%. At this condition, the investment results unprofitable (negative NPV) compared to the reference BtM plant, independently of the electrolyzer cost. If the methanol selling price increases to 600 €/t, the electrolyzer capacity factor

Table 14
Profitability of the plant investment for two different methanol selling prices and electrolyzer investment costs.

Parameter	Value			
Methanol price, €/t	*450*		*600*	
CF_{el}	76.31%		97.75%	
Electricity price, €/MWh (enhanced operation)	33.73		37.73	
Electricity price, €/MWh (baseline operation)	53.86		71.85	
Electrolyzer cost, €/kW	*700*	*400*	*700*	*400*
NPV	−60.79	−24.62	−3.68	32.49
IRR	–	−8.61%	8.93%	24.70%

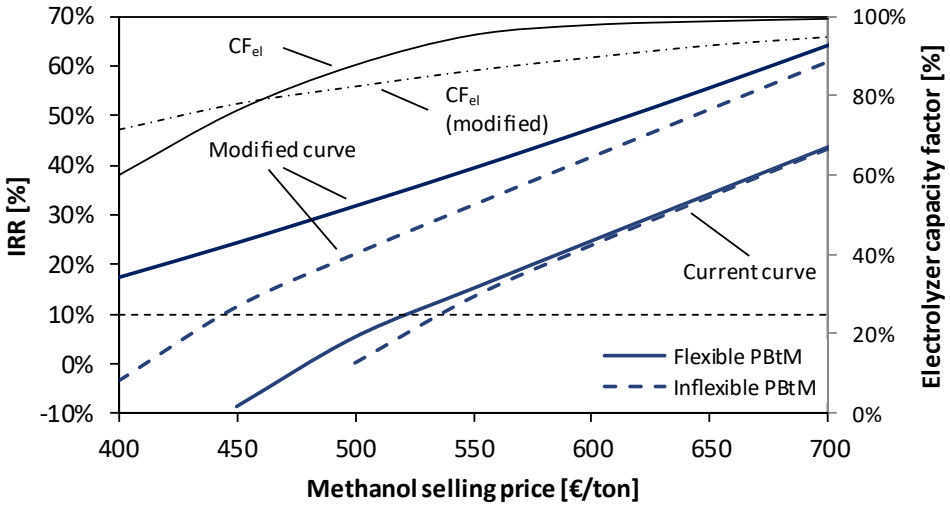

Fig. 12. IRR as a function of the methanol selling price for an electrolyzer investment cost of 400 €/kW. Curves are derived from the two electricity price curves shown in Fig. 11.

increases to 97.8% and the PBtM plant becomes competitive, especially with the low electrolyzer cost.

The results discussed above show that a profitable investment requires high methanol selling price, that involves very high capacity factor. This means that the added value of a flexible PBtM plant is limited compared to an inflexible PBtM plant that always keeps the electrolyzer in operation. However, this result strongly depends on the shape of the cumulative electricity price curve.

In Fig. 12, the IRR is reported as a function of the methanol selling price for an electroylzer investment cost of 400 €/kW. The functions are derived from the 2019 Denmark electricity price curve and from the modified curve. The solid lines refer to the flexible PBtM plant, where the increase of the MeOH selling price involves an increase of the electrolyzer capacity factor, with the method described previously. The dashed lines refer to inflexible plants, with 100% capacity factor of the electrolysis system, purchasing the electricity at the yearly average electricity price of the current price curve (38.5 €/MWh) and of the modified curve (30.4 €/MWh). The IRR value of 10% defines the region above which the PBtM plants is considered profitable with respect to the reference BtM plant.

The curves which derive from the current Danish electricity prices ('current' curve) display profitable investment compared to the BtM route at methanol selling prices higher than about 525 €/t. The curves derived from the modified data show profitable investment compared with the reference option at significantly lower methanol selling prices. This is due to the lower average electricity price of the modified curve with respect to the Denmark one. For both the cases, it can be observed that the solid line is always above the dashed line, meaning that flexible operation of the electrolyzer always leads to a more profitable investment than an inflexible plant. However, with the current electricity price curve, the solid and dashed lines are very close for a wide range of methanol prices, indicating a little advantage of flexible operation. On the contrary, with the modified electricity price curve, the flexible PBtM plant becomes significantly more profitable than the inflexible PBtM plant.

5. Conclusions

This paper assessed, from techno-economic perspectives, different design and operational criteria of Power & Biomass-to-Methanol (PBtM) plants capable to operate flexibly without hydrogen addition (baseline mode) and with hydrogen addition (enhanced mode). Two designs are compared for the methanol synthesis reactor, with different number of tubes, selected either to keep high methanol yield in the enhanced operating mode (enhanced reactor design) or to limit the reactor investment cost (baseline reactor design).

The following main conclusions can be listed from this work:

- Due to the high cost of hydrogen from electrolysis in comparison with the cost of oversizing the methanol synthesis unit, enhanced reactor design is to be preferred over baseline reactor design. Oversizing of the reactor allows significantly higher carbon efficiency in enhanced operating mode (64.4% vs. 59.7%), higher power-to-MeOH efficiency (57.5% vs. 52.3%) and 20% lower cost of the e-MeOH (30.80 vs. 37.76 €/GJ_{LHV}) with the baseline assumptions of this work (i.e. 80% of electrolyzer capacity factor and 2019 Denmark day-ahead market electricity price).
- Due to the high cost of the electrolysis system, competitive cost of the produced e-MeOH can only be achieved with high electrolyzer capacity factors. The impact of increasing the capacity factor from 20% to 80% on the cost of the e-fuel is significantly higher than the impact of a reduction of the electrolyser capital cost, once the pre-requisite of high electrolyzer capacity factor is met. From the modelling work of this paper, a reduction of the cost of the electrolyzer from 700 to 400 €/kW_{el} operating with a capacity factor of 80%, involves a reduction of the LCOe-F by 4.8 €/GJ. On the other hand, increasing the capacity factor from 20 to 80% with an electrolysis cost of 700 €/kW, leads to a reduction of the LCOe-F by about 30 €/GJ.
- The high electrolyzer capacity factor needed to make a PBtM plant economically competitive may reduce the advantage of a plant designed for flexible operations. In fact, with the 2019 Denmark electricity price curve, a limited economic advantage has been calculated for a flexible plant compared to an inflexible plant always operating in enhanced operating mode regardless of the hourly electricity price. Nevertheless, the attractiveness of the flexible plant may increase significantly in future scenarios with very high penetration of intermittent renewables, leading to low average electricity prices, but also longer periods of high peak prices.
- A prerequisite to make PBtM plants economically competitive is that the bio-MeOH and e-MeOH selling price must be sufficiently high to determine high "willingness to pay" price for the electric energy and therefore high electrolyzer capacity factors. With the 2019 Denmark electricity price curve, an e-MeOH selling price higher than about 500 €/t is required.

CRediT authorship contribution statement

Alessandro Poluzzi: Conceptualization, Methodology, Investigation, Formal analysis, Writing – original draft, Visualization, Writing – review & editing, Project administration. **Giulio Guandalini:** Conceptualization, Methodology, Validation, Project administration. **Simone Guffanti:** Methodology, Investigation, Formal analysis (methanol synthesis). **Cristina Elsido:** Methodology, Investigation, Formal analysis (steam cycle optimization). **Stefania Moioli:** Methodology, Investigation, Formal analysis (methanol purification). **Patrick Huttenhuis:** Methodology, Investigation, Formal analysis (capital and operating cost). **Glenn Rexwinkel:** Methodology, Investigation, Formal analysis (capital and operating cost). **Emanuele Martelli:** Validation (steam cycle optimization). **Gianpiero Groppi:** Validation (methanol synthesis). **Matteo C. Romano:** Conceptualization, Supervision, Methodology, Validation, Writing – review & editing, Project administration, Funding acquisition.

Declaration of Competing Interest

The authors declare that they have no known competing financial interests or personal relationships that could have appeared to influence the work reported in this paper.

Acknowledgment

This work was performed within the framework of FLEDGED H2020 Project. This project has received funding from the European Union's Horizon 2020 research and innovation programme under grant agreement No 727600.

Appendix A

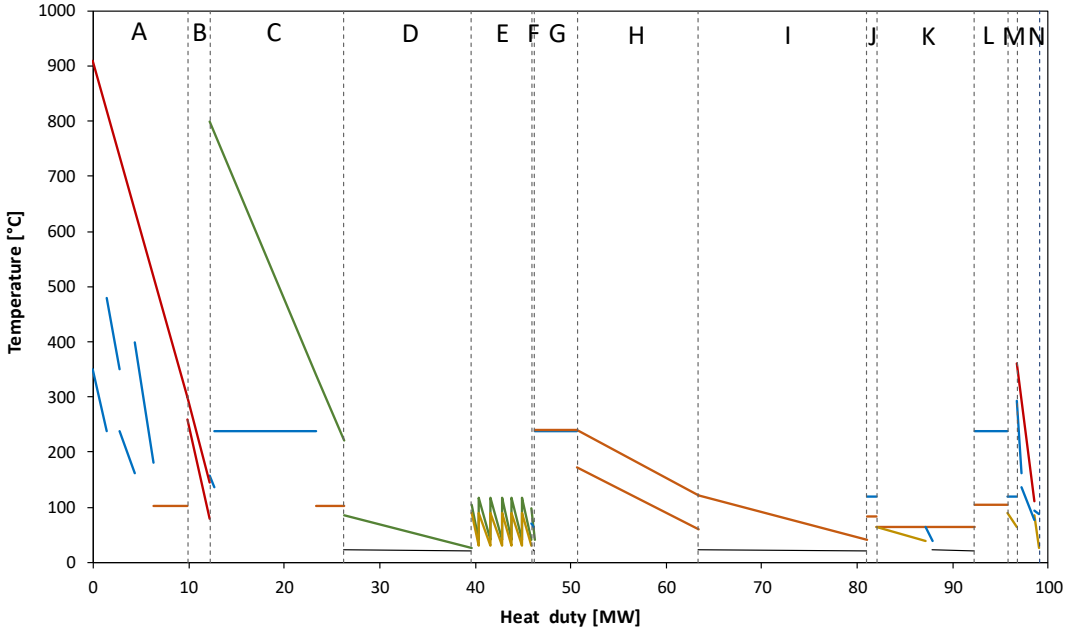

Fig. A1. T-Q diagram of the ERD PBtM plant in enhanced operation. Heat exchangers sections codes are indicated in Table A2.

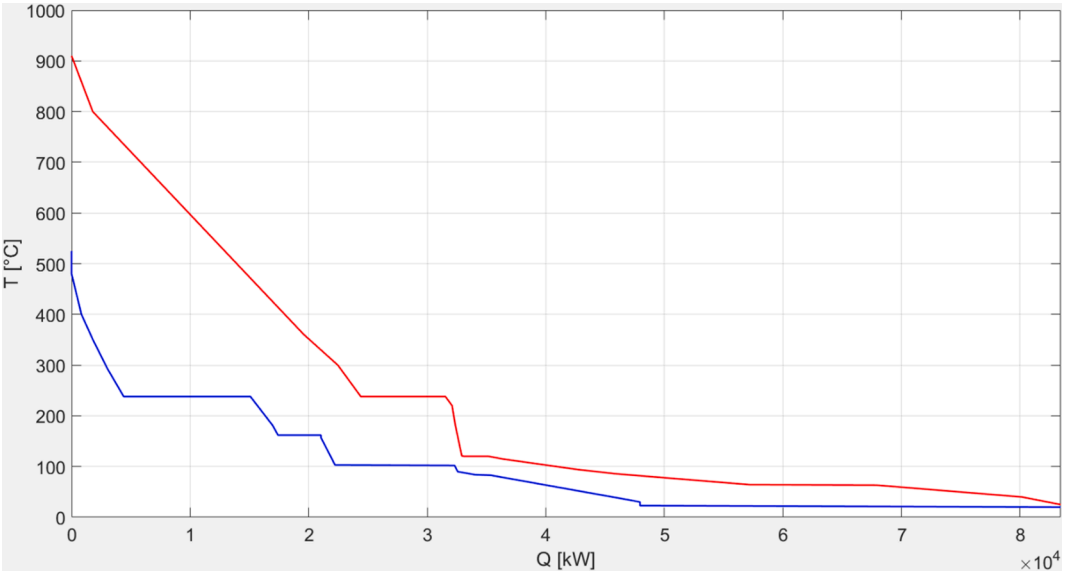

Fig. A2. Grand composite curve of the ERD PBtM plant in enhanced operation.

Table A1
Process modelling assumptions.

Input biomass (as received)	
LHV, MJ/kG_{AR}	9.74
Moisture, $\%_{wt}$	45
Proximate analysis, $\%_{wt,dry}$	
Fixed Carbon	18.84
Volatile matter	80.0
Ash	1.16
Ultimate analysis, $\%_{wt,dry}$	
Carbon	51.19
Hydrogen	6.08
Nitrogen	0.2
Chlorine	0.05
Sulfur	0.02
Oxygen	41.3
Ash	1.16
Biomass pre-treatment	
Biomass moisture at dryer outlet, $\%_{wt}$	15
Biomass temperature at dryer outlet, °C	80
Specific heat consumption, MWh/t_{H2O}	1
Specific power consumption $kWh/t_{bio,dry}$	32
Sorption-enhanced gasification	
Gasifier and combustor pressure, bar	1.43
S/C at gasifier inlet[1]	1.50
Methane content in the syngas, $kg_{CH4}/kg_{bio,dry}$	0.07
Higher hydrocarbon content in the syngas, $kmol_{C2H4}/kmol_{CH4}$	0.25
Fluidizing steam input temperature in enhanced operation, °C	400
Fluidizing steam input temperature in baseline operation, °C	182
Gas injection for sealing and filters, $kg/kg_{bio,dry}$	$H_2O = 0.120Air = 0.031$
Combustor exit temperature, °C	910
Gas superficial velocity at combustor outlet in baseline operation, m/s	5
Oxygen concentration in combustor flue gases, $\%_{mol}$	3
Combustor air temperature in baseline operation, °C	270
Overall pressure drop from combustor to stack, % of gas pressure at valve outlet	4.5
Total solid purge, % of inlet biomass	1
Combustor air fan isentropic/mech.-el efficiency, %	80/94
Loss of solids from the BFB gasifier, % of the circulating solids	0.01
Combustor cyclone separation efficiency, %	Ca: 99.9; Ash:99
Gasifier/combustor thermal losses, % of total thermal input	1.0/1.0
Syngas purification, conditioning and compression	
Reformer exit temperature, °C	800
CH_4 conversion in the reformer, %	90
Oxygen input temperature, °C	25
Oxygen purity, %	100
Syngas temperature at water scrubber inlet, °C	220
Scrubber pump hydraulic/mech.-el efficiency, %	75/90
Electric consumption of the desulfurization unit, $kWh/kg_{H2S,\ removed}$	1.346
Syngas compressor stages	7
Syngas compressor outlet pressure, bar	92
Intercoolers outlet temperature, °C	40
Syngas compressors isentropic/mech.-el. efficiency, %	72/92
Electrolysis efficiency, MW_{LHV}/MW_{el}	0.69
Electrolyzer size, MW	63.29
Electrolysis pressure, bar	30
Methanol synthesis	
Reactor pressure, bar	90
Tube length, m	6
Tube diameter, mm	40
Boiling water temperature, °C	238
Catalyst density, kg/m^3	1712
Catalyst diameter (cylinder), mm	6.0
Catalyst height (cylinder), mm	3.5
Bed voidage degree	0.39
Flash unit temperature, °C	40
Syngas recycle compressor isentropic/mech.-el. efficiency, %	80/94
Methanol purification	
Stabilizing column pressure, bar	1.3
Stabilizing column number of stages	23
Concentration column pressure, bar	1.0
Concentration column number of stages	48
Final product methanol purity, $\%_{wt}$	99.85

[1] The calculation of the S/C includes the fluidization steam, the steam for sealing and cleaning purposes and the moisture of the biomass.

Table A2
Heat sources and sinks of the ERD PBtM plant in enhanced operation.

	Heat sources	Heat sinks
A	SEG combustor flue gas cooler	Superheater MP, Reheater MP, evaporator MP, economizer, superheater LP, concentration column reboiler
B	SEG combustor flue gas cooler	Air preheater
C	Syngas cooler	Economizer, evaporator MP, concentration column reboiler
D	Scrubber water cooler	Cooling water
E	Syngas compressor intercoolers	Belt dryer heat exchanger
F	Hydrogen compressor intercooler	Economizer, cooling water
G	Methanol synthesis reactor	Evaporator MP
H	Methanol cooler	Syngas feed preheater
I	Methanol condenser	Cooling water
J	HRSC condenser	Stabilizing column reboiler
K	Concentration column condenser	Belt dryer heat exchanger, economizer, cooling water
L	HRSC condenser	Concentration column reboiler
M	HRSC condenser	Belt dryer heat exchanger
N	ICE flue gas cooler and hot water production	Superheater LP, economizer, belt dryer heat exchanger

Appendix B

Table B1
Multiplying factors for estimating the total capital investment based on delivered-equipment cost.

	Percent of delivered-equipment cost for *Solid processing plant*	*Solid-fluid processing plant*	*Fluid processing plant*
Direct costs			
Purchased equipment delivered	100	100	100
Purchased-equipment installation	45	39	47
Instrumentation and controls (installed)	18	26	36
Piping (installed)	16	31	68
Electrical systems (installed)	10	10	11
Buildings (including services)	25	29	18
Yard improvements	15	12	10
Service facilities (installed)	40	55	70
Total direct plant cost	269	302	360
Indirect costs			
Engineering and supervision	33	32	33
Construction expenses	39	34	41
Legal expenses	4	4	4
Contractors fee	17	19	22
Contingency	35	37	44
Total indirect plant cost	128	126	144
Fixed-capital investment	397	428	504
Working capital	70	75	89
Total capital investment	467	503	593

Table B2
Parameters for the evaluation of the fixed Opex.

Parameter	Value
Maintenance and repairs, % FCI	5
Operating supplies, % FCI	0.5
Operating labor, % Opex	10
Laboratory costs, % Opex	2.5
Local taxes, % FCI	1
Insurance, % FCI	1
Catalyst cost, €/kg	18.12
Catalyst lifetime, y	4

Appendix C. Supplementary data

Supplementary data to this article can be found online at https://doi.org/10.1016/j.fuel.2021.122113.

References

[1] Directive (EU) 2018/2001 of the European Parliament and of the Council of 11 December 2018 on the promotion of the use of energy from renewable sources. n.d.
[2] Bioenergy IEA. Advanced Biofuels – Potential for Cost Reduction 2020:1–88.
[3] Hannula I. Co-production of synthetic fuels and district heat from biomass residues, carbon dioxide and electricity: Performance and cost analysis. Biomass Bioenergy 2015;74:26–46. https://doi.org/10.1016/j.biombioe.2015.01.006.
[4] Hannula I. Hydrogen enhancement potential of synthetic biofuels manufacture in the European context: A techno-economic assessment. Energy 2016;104:199–212. https://doi.org/10.1016/j.energy.2016.03.119.
[5] Koponen K, Hannula I. GHG emission balances and prospects of hydrogen enhanced synthetic biofuels from solid biomass in the European context. Appl Energy 2017;200:106–18. https://doi.org/10.1016/j.apenergy.2017.05.014.
[6] Albrecht FG, König DH, Baucks N, Dietrich RU. A standardized methodology for the techno-economic evaluation of alternative fuels – A case study. Fuel 2017;194:511–26. https://doi.org/10.1016/j.fuel.2016.12.003.
[7] Hillestad M, Ostadi M, Alamo Serrano Gd, Rytter E, Austbø B, Pharoah JG, et al. Improving carbon efficiency and profitability of the biomass to liquid process with hydrogen from renewable power. Fuel 2018;234:1431–51. https://doi.org/10.1016/j.fuel.2018.08.004.
[8] Zhang H, Wang L, Van herle J, Maréchal F, Desideri U. Techno-economic evaluation of biomass-to-fuels with solid-oxide electrolyzer. Appl Energy 2020;270:115113. https://doi.org/10.1016/j.apenergy.2020.115113.
[9] Koytsoumpa EI, Karellas S, Kakaras E. Modelling of methanol production via combined gasification and power to fuel. Renew Energy 2020;158:598–611. https://doi.org/10.1016/j.renene.2020.05.169.
[10] Edwards R, Larivé J-F, Rickeard D, Weindorf W. Well-to-tank Report Version 4.a. JEC well-to-wheels analysis 2014. Doi: 10.2790/95629.
[11] Martínez I, Romano MC. Flexible sorption enhanced gasification (SEG) of biomass for the production of synthetic natural gas (SNG) and liquid biofuels: Process assessment of stand-alone and power-to-gas plant schemes for SNG production. Energy 2016;113:615–30. https://doi.org/10.1016/j.energy.2016.07.026.
[12] Pitkäoja A, Ritvanen J, Hafner S, Hyppänen T, Scheffknecht G. Simulation of a sorbent enhanced gasification pilot reactor and validation of reactor model. Energy Convers Manag 2020;204:112318. https://doi.org/10.1016/j.enconman.2019.112318.
[13] Hawthorne C, Poboss N, Dieter H, Gredinger A, Zieba M. Operation and results of a 200-kW th dual fluidized bed pilot plant gasifier with adsorption-enhanced reforming 2012. Doi: 10.1007/s13399-012-0053-3.
[14] Pfeifer C, Puchner B, Hofbauer H. Comparison of dual fluidized bed steam gasification of biomass with and without selective transport of CO2. Chem Eng Sci 2009;64(23):5073–83. https://doi.org/10.1016/j.ces.2009.08.014.
[15] van Leeuwen C, Mulder M. Power-to-gas in electricity markets dominated by renewables. Appl Energy 2018;232:258–72. https://doi.org/10.1016/j.apenergy.2018.09.217.
[16] Echt B, Leppin D, Mamrosh D, Mirdadian D, Seeger D, Warren B. Fundamentals of Low-Tonnage Sulfur Removal and Recovery 2017:1–90.
[17] Pröll T, Hofbauer H. H2 rich syngas by selective CO2 removal from biomass gasification in a dual fluidized bed system - Process modelling approach. Fuel Process Technol 2008;89(11):1207–17. https://doi.org/10.1016/j.fuproc.2008.05.020.
[18] W.a. Amos, Report on Biomass Drying Technology Report on Biomass Drying Technology SAE Trans 1998;106:475–485. https://doi.org/NREL/TP-570-25885.
[19] Fagernäs L, Brammer J, Wilén C, Lauer M, Verhoeff F. Drying of biomass for second generation synfuel production 2010;34:1267–77. Doi: 10.1016/j.biombioe.2010.04.005.
[20] STELA drying technology brochure on low-temperature belt dryer. Brochure on Low-temperature belt dryer n.d.
[21] Martínez Ana, Pröll Tobias, Romeo Luis M. Lime enhanced biomass gasification. Energy penalty reduction by solids preheating in the calciner. Int J Hydrogen Energy 2012;37(20):15086–95. https://doi.org/10.1016/j.ijhydene.2012.08.002.
[22] Fuchs J, Schmid JC, Müller S, Mauerhofer AM, Benedikt F, Hofbauer H. The impact of gasification temperature on the process characteristics of sorption-enhanced reforming of biomass. Biomass Convers Biorefinery 2020;10(4):925–36. https://doi.org/10.1007/s13399-019-00439-9.
[23] Grasa Gemma S, Abanades J Carlos. CO2 Capture Capacity of CaO in Long Series of Carbonation/Calcination Cycles. Ind Eng Chem Res 2006;45(26):8846–51. https://doi.org/10.1021/ie0606946.
[24] Loffler G, Kaiser S, Bosch K, Hofbauer H. Hydrodynamics of a dual uidized-bed gasiÿer — Part I : simulation of a riser with gas injection and diffuser 2003;58:4197–213. Doi: 10.1016/S0009-2509(03)00232-X.
[25] Proll T, Hofbauer H. Int. J. Chem. Development and Application of a Simulation Tool for Biomass Gasification Based Processes Tobias Proll 2008;6.
[26] Energie- VDF, Biotechnik V-, Poboß N. Experimentelle Untersuchung der sorptionsunterstützten Reformierung; 2016.
[27] Armbrust N, Schweitzer D, Gredinger A, Beirow M, Poboss TBN, Hawthorne C, et al. Gasification of Biomass with In-Situ CO 2 Capture and Separation in a 200 kW th Pilot Plant Fluidized bed gasification infrastructure; 2014.
[28] Schmid JC, Fuchs J, Benedikt F, Mauerhofer AM. Sorption enhanced reforming with the novel dual fluidized bed; 2017.
[29] Koppatz S, Pfeifer C, Rauch R, Hofbauer H, Marquard-moellenstedt T, Specht M. H 2 rich product gas by steam gasi fi cation of biomass with in situ CO 2 absorption in a dual fl uidized bed system of 8 MW fuel input. Fuel Process Technol 2009;90:914–21. https://doi.org/10.1016/j.fuproc.2009.03.016.
[30] Alamia Alberto, Òsk Gardarsdòttir Stefania, Larsson Anton, Normann Fredrik, Thunman Henrik. Efficiency Comparison of Large-Scale Standalone, Centralized, and Distributed Thermochemical Biorefineries. Energy Technol 2017;5(8):1435–48. https://doi.org/10.1002/ente.201600719.
[31] Hafner S, Schmid M, Scheffknecht G. Parametric Study on the Adjustability of the Syngas Composition by Sorption-Enhanced Gasification in a Dual-Fluidized Bed Pilot Plant. Energies 2021;14(2):399.
[32] Hafner S, Spörl R, Scheffknecht G. Sorption Enhanced Gasification: Process validation and investigations on the syngas composition in a 200 kWth dual fluidized bed facility. Conf. Proc. 23rd Int. Conf. FBC, Seoul, South Korea: 2018, p. 826–832.
[33] Hafner S, Schmid M, Spörl R, Scheffknecht G. Experimental Investigation of the Sorption Enhanced Gasification of Biomass in a Dual Fluidized Bed Pilot Plant. Proc. 27th Eur. Biomass Conf., Lisbon (Portugal): n.d., p. 2019.
[34] Hafner S, Schmid MWP. 3 – Deliverable D3.4: Final experimental results on SEG process experiments at pilot (TRL5). scale for stationary and flexible operating regimes. 2020.
[35] Kurkela E, Kurkela M, Frilund C, Hiltunen I, Rollins B, Steele A. Flexible Hybrid Process for Combined Production of Heat, Power and Renewable Feedstock for Refineries: Managing seasonal energy supply and demand for heat and power in Europe. Johnson Matthey Technol Rev 2021;65:346–8. https://doi.org/10.1595/205651321X16158839334031.
[36] Kurkela E, Kurkela M, Hiltunen I. Steam-oxygen gasification of forest residues and bark followed by hot gas filtration and catalytic reforming of tars: Results of an extended time test. Fuel Process Technol 2016;141:148–58. https://doi.org/10.1016/j.fuproc.2015.06.005.
[37] Hannula I, Kurkela E. Liquid transportation fuels via large-scale fluidised bed gasification of lignocellulosic biomass; 2013.
[38] Kazemi Abolghasem, Malayeri Mojtaba, Gharibi kharaji Abolfazl, Shariati Ahmad. Feasibility study, simulation and economical evaluation of natural gas sweetening processes - Part 1: A case study on a low capacity plant in iran. J Nat Gas Sci Eng 2014;20:16–22. https://doi.org/10.1016/j.jngse.2014.06.001.
[39] Bussche KMVanden, Froment GF. A Steady-State Kinetic Model for Methanol Synthesis and the Water Gas Shift Reaction on a Commercial Cu/ZnO/Al2O3Catalyst. J Catal 1996;161(1):1–10. https://doi.org/10.1006/jcat.1996.0156.
[40] Montebelli A, Visconti CG, Groppi G, Tronconi E, Ferreira C, Kohler S. Enabling small-scale methanol synthesis reactors through the adoption of highly conductive structured catalysts. Catal Today 2013;215:176–85. https://doi.org/10.1016/j.cattod.2013.02.020.
[41] Twigg Martyn V, Spencer Michael S. Deactivation of supported copper metal catalysts for hydrogenation reactions. Appl Catal A Gen 2001;212(1-2):161–74. https://doi.org/10.1016/S0926-860X(00)00854-1.
[42] Zatti M, Gabba M, Rossi M, Morini M, Gambarotta A, Martelli E. Towards the optimal design and operation of multi-energy systems: the “efficity” project 2018;17:2409–19.
[43] Elsido C, Martelli E, Grossmann IE. Multiperiod Optimization of Heat Exchanger Networks with Integrated Thermodynamic Cycles and Thermal Storages. Submitt to Comput Chem Eng n.d.
[44] Elsido C, Martelli E, Grossmann IE. Simultaneous Multiperiod Optimization of Rankine Cycles and Heat Exchanger Networks. Comput Aided Chem Eng 2020;48:1495–500.
[45] Martelli E, Elsido C, Mian A, Marechal F. MINLP model and two-stage algorithm for the simultaneous synthesis of heat exchanger networks, utility systems and heat recovery cycles. Comput Chem Eng 2017;106:663–89. https://doi.org/10.1016/j.compchemeng.2017.01.043.
[46] Elsido C, Mian A, Martelli E. A systematic methodology for the techno-economic optimization of Organic Rankine Cycles. Energy Procedia 2017;129:26–33. https://doi.org/10.1016/j.egypro.2017.09.171.
[47] Elsido C, Martelli E, Grossmann IE. A bilevel decomposition method for the simultaneous heat integration and synthesis of steam/organic Rankine cycles. Comput Chem Eng 2019;128:228–45. https://doi.org/10.1016/j.compchemeng.2019.05.041.
[48] Yee TF, Grossmann IE. Simultaneous optimization models for heat integration—II. Heat exchanger network synthesis. Comput Chem Eng 1990;14(10):1165–84.

[49] Elsido C, Martelli E, Kreutz T. Heat integration and heat recovery steam cycle optimization for a low-carbon lignite/biomass-to-jet fuel demonstration project. Appl Energy 2019;239:1322–42. https://doi.org/10.1016/j.apenergy.2019.01.221.
[50] Poluzzi Alessandro, Guandalini Giulio, Romano Matteo C. "Potential carbon efficiency" as a new index to track the performance of biofuels production processes. Biomass Bioenergy 2020;142:105618. https://doi.org/10.1016/j.biombioe.2020.105618.
[51] Schmidt O, Gambhir A, Staffell I, Hawkes A, Nelson J, Few S. Future cost and performance of water electrolysis: An expert elicitation study. Int J Hydrogen Energy 2017;42(52):30470–92. https://doi.org/10.1016/j.ijhydene.2017.10.045.
[52] Bertuccioli L, Chan A, Hart D, Lehner F, Madden B, Standen E. Development of water electrolysis in the European Union - Final report. FCH-JU 2014.
[53] Queneau PE, Marcuson SW. Oxygen Pyrometallurgy at Copper Cliff-A Half Century of Progress; 1996.
[54] Kreutz T, Williams R, Consonni S, Chiesa P. Co-production of hydrogen, electricity and CO2 from coal with commercially ready technology. Part B: Economic analysis. Int J Hydrogen Energy 2005;30:769–84. https://doi.org/10.1016/j.ijhydene.2004.08.001.
[55] entsoe Transparency Platform n.d.
[56] International Energy Agency. The Future of Hydrogen - Seizing today's opportunities - Report prepared for the G20, Japan; 2019.
[57] Tan Eric CD, Talmadge Michael, Dutta Abhijit, Hensley Jesse, Snowden-Swan Lesley J, Humbird David, et al. Conceptual process design and economics for the production of high-octane gasoline blendstock via indirect liquefaction of biomass through methanol/dimethyl ether intermediates. Biofuels, Bioprod Biorefining 2016;10(1):17–35.
[58] Blanco H, Nijs W, Ruf J, Faaij A. Potential for hydrogen and Power-to-Liquid in a low-carbon EU energy system using cost optimization. Appl Energy 2018;232:617–39. https://doi.org/10.1016/j.apenergy.2018.09.216.
[59] Sorknæs P, Lund Henrik, Skov IR, Djørup S, Skytte K, Morthorst PE, et al. Smart Energy Markets - Future electricity, gas and heating markets. Renew Sustain Energy Rev 2020;119:109655. https://doi.org/10.1016/j.rser.2019.109655.
[60] Ruhnau O. Market-based renewables: How flexible hydrogen electrolyzers stabilize wind and solar market values; 2020.
[61] Seel J, Mills A, Wiser R, Deb S, Asokkumar A, Hassanzadeh M, et al. Impacts of High Variable Renewable Energy Futures on Wholesale Electricity Prices, and on Electric-Sector Decision Making; 2018.
[62] Afman M, Hers S, Scholten T. Energy and electricity price scenarios 2020–2023-2030. Input to Power to Ammonia value chains and business cases. 2017.